UiT
THE ARCTIC
UNIVERSITY
OF NORWAY

Department of Physics and Technology

Investigation of Thermo-Optical Phase Modulator for Chip Based Structured Illumination Microscopy

—

Sourov Kumar Das

FYS-3900 Master's Thesis in Physics, November 2018

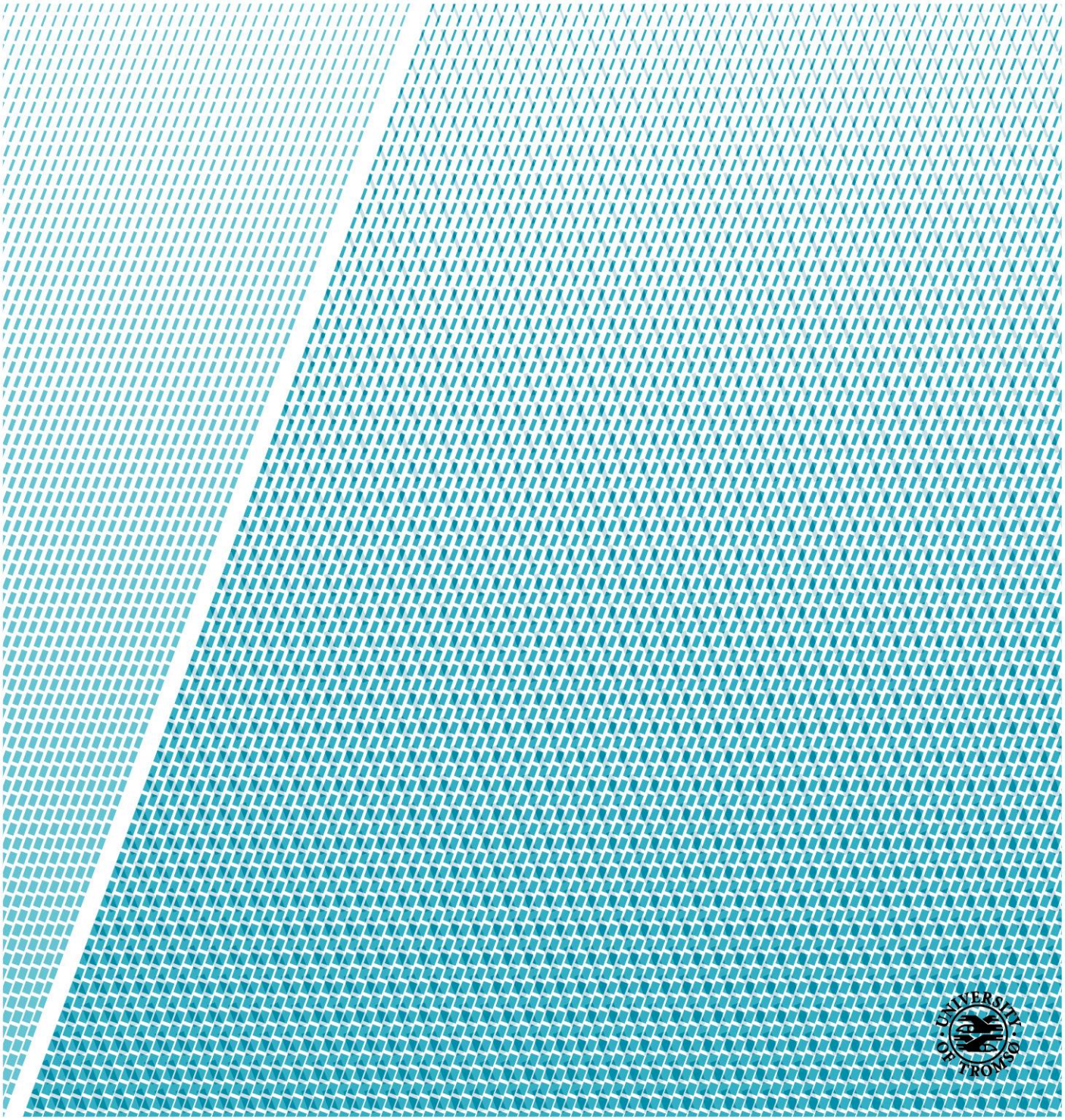

Acknowledgements

I would first like to thank my thesis supervisor Prof. Balpreet Singh Ahluwalia and co-supervisors Dr. Firehun Tsige Dullo and Dr. Anowarul Habib. They have provided me with unfailing support and continuous encouragement throughout the process of researching and writing this thesis. This accomplishment would not have been possible without them. Thank you.

I would like to thank all the fellow researcher at the Optics Group, who shared their valuable knowledge and have made comments suggestions on my paper which gave me an inspiration to improve the quality of the thesis.

Finally, I thank my parents for providing a good education and supporting me along the way.

Abstract

Optical nanoscopy is an emerging field and enables super-resolution of biological cells. Among the existing nanoscopy techniques, structured illumination microscopy (SIM) is most promising candidate for live cell imaging due to its high-imaging speed, limited photo-toxicity and its suitability with most commonly used fluorophore. One of research focus of the optics group at the department is to develop photonic-chip based SIM.

For SIM it is essential to perform phase stepping. This thesis involves developing a protocol for fabricating and investigation of on-chip polymer based phase modulator for SIM-on-chip. From our experimental result we can conclude that, fabrication of a polymer-based phase modulator is achievable using lift-off method. The entire fabrication process was optimized locally at UiT.

The phase response of on-chip polymer based phase modulator is fast, has sufficient visibility and repeatable over time. I have also demonstrated three equidistant phase stepping as required for SIM imaging.

This thermo-optics chip was designed with smaller interference angels ($20° \; and \; 30°$) to be able to capture the interference fringe patterns. We observed that a 60x, 1.2NA objective lens is needed to capture the interference fringes. The experimental results of fringe spacing show good agreement with the analytical results.

Some limitation of using the polymer based thermos-optic phase modulation was also observed. One of them is the cross-heating. Experiment shows that for chosen chip continuous phase modulation time should be limited to 15 seconds, after 15 seconds phase shift measurements might not be reliable. After 15 seconds, both the arms of the waveguides are heated and the phase difference reduces.

From the experimental results, required power for a π shift using 640 nm, TM mode is 185mW and for 561nm, TM mode it is 230mW. In TM mode phase starts to change with as little as 20mW power. The low power for TM mode also means that the chip will not be heated up so much, which is advantageous for live cell imaging. Whereas, For TE mode phase shift starts at a higher power (≈ 150mW) and total power required for one π shift is considerably more than TM mode. At higher power cross-heating happens much faster.

From phase change according to the length experiment, we observed that for 1cm length arm, phase shift starts at ≈ 300mW, but the total power it takes for one π shift is approximately half of the power that is needed for 0.5 cm.

Considering all these results, we can suggest that for an ideal SIM chip, one should use 640nm, TM mode in combination with shortest possible heat sensing length.

Contents of the thesis

List of Figures

List of abbreviations

- SIM: Structured Illumination Microscopy
- PDMS: Polydimethylsiloxane
- CMDR: CellMask Deep Red
- CMO: CellMask Orange
- WEC: Wedge Error Compensation
- DI: Distilled Water
- ICP: Inductively Coupled Plasma
- IPA: Isopropyl Alcohol
- CTE: Coefficient of Thermal Expansion
- PAA: Poly (acrylic acid)

1 Motivation

Before I started this master project, the optics group at the department have been working on waveguide chip-based structured illumination microscopy (SIM). Chip-based SIM in principle can produce higher resolution, it is highly compact and most likely cheaper relative to commercially available SIM.

SIM provide resolution enhancement of factor two. To achieve this the target is illuminated with an interference fringes instead of a uniform illumination. In SIM, the interference fringes in three different angles (orientations) and three (five) phase steps per angle is required for two (three) dimensional SIM. Thus in total 9 (15) images are acquired for 2D (3D). There are many ways of generating phase stepping for chip-based SIM. When I joined the project, most of the study for chip-based SIM was based on using on-chip phase modulation, where 9 input waveguides were used to provide phase shifting. The design was not only complicated but it also had no freedom to change the phase once the waveguide chip is fabricated. On-chip phase stepping using 9 waveguides had too many waveguide crossing, bends and long structures resulting on high propagation losses. Before, I joined the group, on-chip phase stepping was not working appropriately.

In this thesis, I have investigated phase stepping using on-chip thermo-optical phase modulator, using PDMS. To perform on-chip thermo-optical phase shift, the fabrication process had to be optimized locally at the department. The waveguide chips were fabricated in Barcelona and had openings in the cladding for phase modulation. However, the entire fabrication process for on-chip thermo-optical phase modulator had to be optimized as no prior experience on such fabrication was carried out in the group. To do this, first I received cleanroom training at the department. Several fabrication challenges were encountered and solved systematically. Finally, I managed to fabricate waveguides with functional on-chip thermo-optic phase modulation. I have spent more than 70% of my time in this thesis in fabrication process leaving little time for the characterization of the waveguide chips. Nevertheless, I have obtained the preliminary experimental results for on-chip thermo-optical phase modulator that I will present in this work. These results will show that, phase response is fast, has sufficient visibility, phase shift is repeatable over time and phase stepping is achieved for SIM imaging. The on-chip phase modulation takes as little as $185mW$ for a full π shift.

The main advantage of phase-stepping using on-chip thermo-optical phase modulator is it reduces the number of input waveguides to 3 or less and the design is less complicated and most importantly gives complete flexibility to opt for the desirable phase shift.

2 Theory and background

2.1 Conventional vs chip-based Structured Illumination Microscopy

The Structured illumination microscopy is one of the most rapidly growing fluorescence microscopy technique which can go beyond the diffraction limit using conventional microscopes. The fundamental limit in light microscopy is limited by the wavelength of light and light gathering power of the objective lens. This is known as abbe diffraction limit:

$$d = \frac{\lambda}{2n \sin\theta} = \frac{\lambda}{2NA} \qquad (2.1)$$

Where n is the refractive index of the medium and N.A. is numerical aperture of the objective lens. A point spread function in spatial domain is represented by an optical transfer function in frequency domain. Fig 2.1 (a) shows an optical transfer function of an objective lens, red circle indicates the diffraction limit in frequency domain, which is known as cut-off frequency. The smaller the objects is, the more is the diffraction. In frequency domain this corresponds to higher frequency. The two red crosses in Fig 2.1 (a) highlight that these frequency is outside the cut-off frequency of the objective lens. In SIM microscopy this diffraction limited object is illuminated with a structured pattern, of known frequency (period). This leads to mixing of two spatial frequencies (illumination and sample) creating new patterns containing up-conversion (high frequency) and down-conversion (low frequency) components. Net effect of this can be seen as Fig 2.1 (b). The lower frequency components which are within the cut-off frequency of the objective lens can then be imaged. By imaging this new pattern and using the known high frequency illumination pattern it is possible to resolve the diffraction limited object.

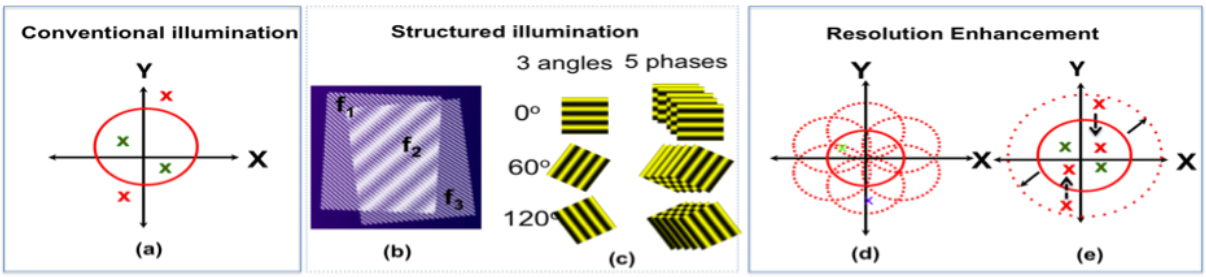

Figure 2.1 Working principle of structured illumination microscopy (a) Optical transfer function of the lens with cut-off frequency. (b) Formation of lower frequency fringes by interfering higher frequency signals. (c) For 3D SIM, images are acquired for 3 angles and 5 phases. (d-e) The enhancement in optical resolution is obtained by pushing higher frequencies inside OTF cut-off. (Image taken from Ahluwalia's ERC project)

In SIM, illumination patterns in three different angles (orientations) and three (five) phase steps per angle is required for two (three) dimensional SIM, as shown in Fig 2.1 (c). These illumination patterns are created by an objective lens. The NA of this objective lens defines the spacing between these patterns. The resolution of SIM depends on how closely we can place the interference fringes. As the objective lens used to generate the illumination pattern is diffraction limited, it cannot generate fringes smaller than the diffraction limit itself. Therefore, SIM can achieve a resolution enhancement of a factor of 2 using this patterns. Which is approximately

$$d_{sim} = \frac{\lambda}{4NA} \qquad (2.2)$$

In the Optics group, the research is focused towards the development of SIM on-chip. In SIM-on-chip the illumination pattern is generated by the evanescent standing waves created by two opposing waveguide. Spacing of the fringe patterns created by SIM on-chip is a function of effective refractive index of the propagating mode (n_{eff}) and the angle of interference (α). Resolution limit of SIM on-chip can be expressed as:

$$d_{on-chip} = \frac{\lambda}{4\, n_{eff}\, sin(\alpha/2)} \qquad (2.3)$$

At 180-degree interference angle resolution only depends on the effective refractive index of the propagating mode (n_{eff}).

$$d_{on-chip} = \frac{\lambda}{4\, n_{eff}} \qquad (2.4)$$

Objective with immersion media can have NA as large as 1.4. But for SIM on-chip used this thesis has and n_eff of around 1.72 (for our waveguide material). Therefore, SIM on-chip can achieve better resolution than conventional SIM.

There are three different ways the phase stepping can be performed for SIM-on-chip.

On chip phase stepping: the phase difference between the 3 waveguide combinations is because of the path length difference between the waveguides for those combinations. One waveguide is active at a time and 3 waveguides are needed for achieving 3 phase steps, Fig 2.2 (a)

Off-chip phase stepping: the phase shift can be introduced by changing the phase shift between one of the waveguide arm before coupling light into the waveguide, one such example is changing the temperature of one of the input coupling fibres. In this case two waveguides have to be active simultaneously to generate the interference fringes, Fig 2.2 (b)

On-chip thermo-optic phase stepping: One only waveguide is used and the light is split into two arms and are then interference in counter-propagating direction. Here the phase change is as a result of a refractive index change due to temperature variation in one of the waveguide arm Fig 2.2 (c)

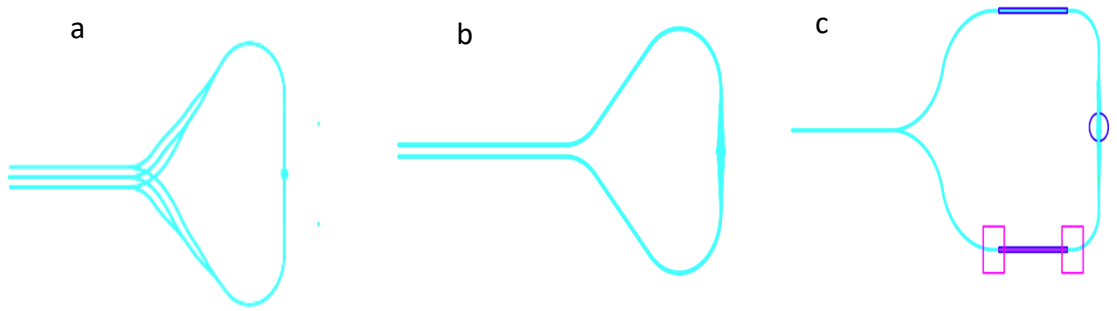

Figure 2.2 Chip based SIM (a) on-chip phase SIM structure (b) off-chip phase modulator SIM structure and (c) thermo-optic based phase modulator SIM structure. These designs are only for one orientation. The angle between the interfering waveguides is 180 degree.

2.2 Total internal reflection and evanescent field

Refractive index of a media is defined as $n = c/v$. When a ray of light travels from a media with higher refractive index, n_1 to a media with lower refractive index,n_2, some of the light gets reflected from the boundary between the two media and some of it gets refracted (transmitted). This refracted ray makes an angle θ_2 with the normal Fig 2.1 (a)[2]. Angle of refraction θ_2 is related to the angle of incidence θ_1 by Snell's law:

$$n_1 sin\theta_1 = n_2 sin\theta_2 \qquad (2.5)$$

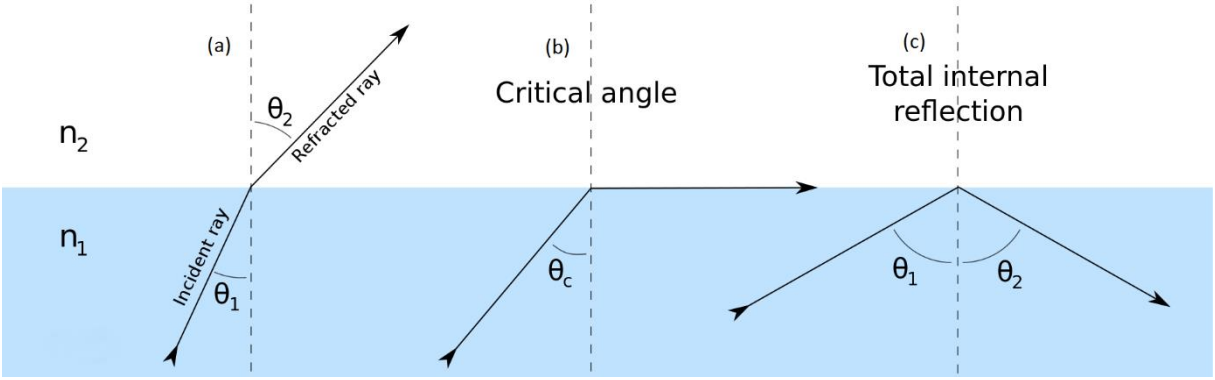

Figure 2.3 Relation between the angles of incidence and refraction (a) ray of light travels from a media with higher refractive index n_1 to a lower refractive index media n_2. ($\theta_2 > \theta_1$) (b) refracted ray reaches 90° when the incident ray reaches critical angle (θ_c) (c) incident angle is larger than the critical angle ($\theta_1 > \theta_c$) and the ray is totally reflected

As the angle of incidence increases, refracted ray bends away from normal. When it reaches critical angle, $\theta_1 = \theta_c$, refracted ray becomes 90°, Fig 2.1(b).

$$n_1 sin\theta_c = n_2 \sin(90°)$$

$$\theta_c = sin^{-1}\frac{n_2}{n_1} \qquad (2.6)$$

No refraction occur when the incident angle become larger than the critical angle ($\theta_1 > \theta_c$), and the incident ray gets totally reflected back to its original media. This phenomenon is called total internal reflection (TIR). Propagation of light in an optical waveguide follow this principle, Fig 2.3 [3].

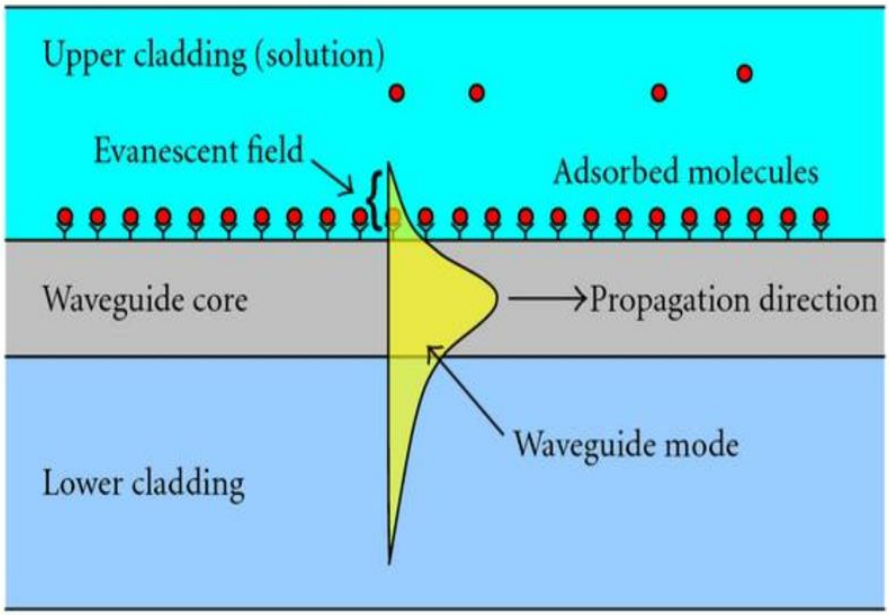

Figure 2.4 Evanescent field generation inside a waveguide

Incident light gets internally reflected at each boundary propagates forward. But not all the light is reflected, some of the light leaks out from the from the waveguide core and penetrates into the cladding media. This penetrating light is called the evanescent field. The distance at which the intensity of the electromagnetic field drops to 1/e of its value at the interface is known as penetration depth d_{ev} .

$$d_{ev}(i) = \frac{1}{\sqrt{n_{eff}^2 - n_i^2}\, k_0} \qquad (2.7)$$

Where n_{eff} is the effective refractive index of the propagating mode, n_i is the refractive index of the of the top or bottom cladding, $k_0 = 2\pi/\lambda_0$, is the wavenumber where λ_0 is the wavelength.

2.3 Interference of two monochromatic waves

Interference of two monochromatic waves with complex amplitudes produce another monochromatic wave. The resultant wave has the same frequency and a complex amplitude. Interference of two monochromatic waves $U_1(r)$ and U_2 can be written as:

$$U(r) = U_1(r) + U_2(r) \qquad [4]$$

Optical intensity of a monochromatic wave is the absolute square of its complex amplitude. Intensity of the two waves are,$I_1 = |U_1|^2 \; and \; I_2 = |U_2|^2$, and the total intensity:

$$I = |U|^2 = |U_1 + U_2|^2 = |U_1|^2 + |U_2|^2 + U_1^* U_2 + U_1 U_2^* \qquad (2.8)$$

Substituting, $U_1 = \sqrt{I_1}\exp(j\varphi_1) \; and \; U_2 = \sqrt{I_2}\exp(j\varphi_2)$ in Eq. 2.3

$$I = I_1 + I_2 + 2\sqrt{I_1 I_2}\cos(\varphi_2 - \varphi_1)$$

$$I = I_1 + I_2 + 2\sqrt{I_1 I_2}\,cos(\varphi) \qquad (2.9)$$

$$\varphi = \varphi_2 - \varphi_1, Phase\; difference$$

Equation (2.4) is called the ***interference equation.*** Value of the phase difference can either be positive or negative. When the value is positive it's called a constructive interference and when negative its destructive interference. If both of the wave has same intensity, $I_1 = I_2 = I_0$ Eq. 2.4 becomes

$$I = 2I_0(1 + cos\varphi) = 4I_0\, cos^2(\varphi/2) \qquad (2.10)$$

So for no phase difference between two waves, the total intensity becomes 4 times larger $\varphi = 0, I = 4I_0$ and when they are 180 degree out of phase the total intensity is,$\varphi = \pi, I = 0$.

3 Fabrication of the thermo-optical phase modulator

3.1 Chip design

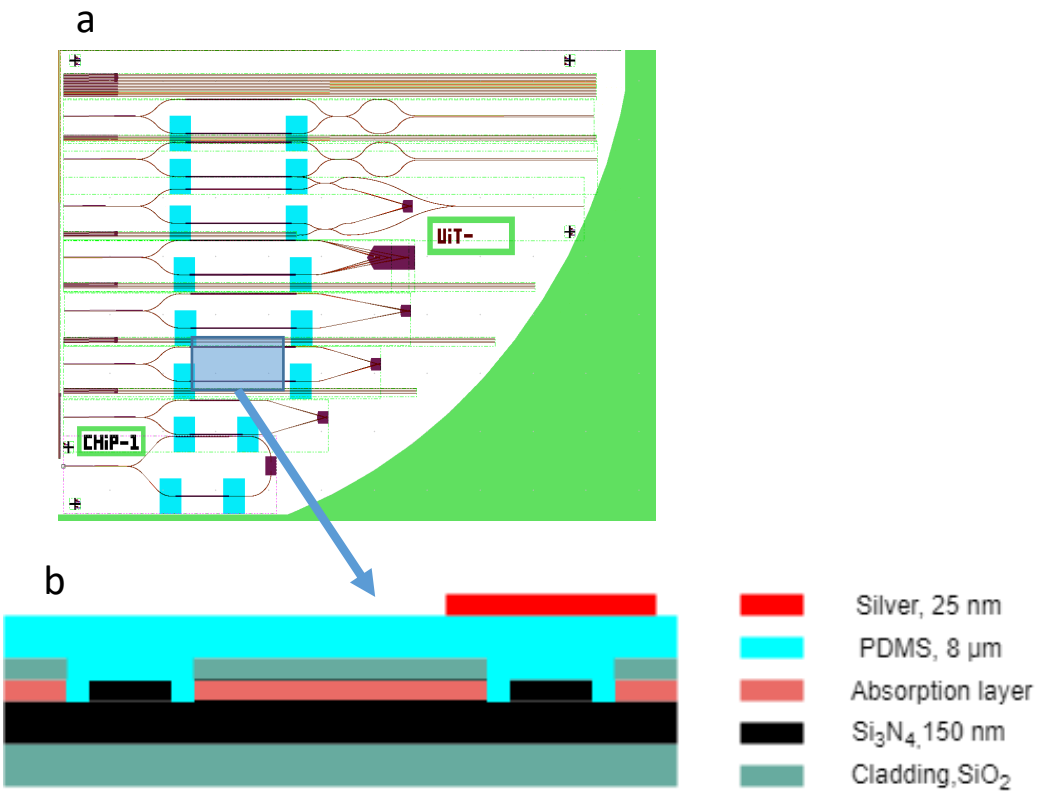

Figure 3.1 Thermo-optics chip. (a) Design of the chip (b) shows how the cross section would look like after this fabrication process

This thermo-optics chip was designed by my co-supervisor Dr. Firehun Tsige Dullo and fabricated in Barcelona. I was involved in developing the lift-off protocol for fabricating the micro heaters on PDMS and taking the phase shift measurements. Working principle of this chip will be discussed in phase measurements chapter.

3.2 Literature review

In my thesis, I have focused on three research papers that have developed fabrication process of thermo-optical modulation using PDMS. The three papers presented below, discusses three different approach of fabricating micro heaters on PDMS. The key methods are respectively lift-off, wet etching and modifying PDMS as a heating element.

3.2.1 Guo and DeWeerth - 2010

This paper presents a method for patterning gold microstructures on a PDMS substrate. Guo and DeWeerth [5] were able to produce gold lines as small as $10\ \mu m$ wide using negative photoresist (SU-8) and lift-off technique. Cured SU-8 is very hard to remove. They overcome this problem by using a thin layer ($400nm$) of PAA (Poly (acrylic acid)) as a sacrificial layer between the photoresist and PDMS. PAA is a water-soluble polymer but insoluble in SU-8 developer, so it was not affected during the developing process. Oxygen plasma is used for PDMS-PAA bonding. They have also encountered the problem of photoresist cracking which was solved by ramping temperature up and down during the baking steps.

3.2.2 Adrega and Lacour - 2010

In this paper similar work is reported by Adrega and Lacour[6]. They have used an alternative method of fabrication, positive photoresist (AZ 1505 by MicroChem) and wet etching. The whole fabrication process was carried out in low-temperature process (below $75\ °C$). Gold has poor adhesion to PDMS, $3nm$ thick chromium layer is used as an adhesion layer between $70\ \mu m$ PDMS and $40nm$ gold conductors. After development, chromium/gold/chromium layer is wet etched. The photoresist strip is performed by UV flood exposure, followed by immersion in photoresist developer. They have not seen any photoresist crack after developing. However, sub-micron cracks were observed on gold surface after film deposition. They hypothesized that it caused due to the large mismatch of thermal expansion coefficients of PDMS and gold.

3.2.3 Chuang and Wereley - 2008

Chuang and Wereley propose [7] a completely different approach of fabrication. Instead of fabricating heating element on PDMS film, PDMS prepolymer can be modified as a heating element simply by mixing it with a metallic powder. A piece of pre-moulded PDMS is used as the substrate material and a mixture of PDMS and copper as the conducting element. The mixture is poured into the PDMS mould and the excess mixture is gently removed using a razor blade. The mixture was cured on a hotplate for 1 hour at$100°\ C$. They were able to achieve $92°C$ using power as low as 210mW.

Summary: My thesis work involves a combination of the first 2 papers, lift-off using positive photoresist. The third method from Chuang ad Wereley was considered as an alternative approach but this method would be ineffective, because conductive PDMS is not transparent.

3.3 Methods of fabricating micro heaters on Chip

There are many methods of patterning microstructures on a substrate, namely lift-off[5], wet etching[8], shadow masking[9], printing/stamping[10]. Fabrication lab at UiT-The Arctic University of Norway facilitates apparatus for wet etching and lift-off processes.

In wet etching, a target material for example a metal is deposited to a substrate in the form of a thin layer. Then using a photoresist mask and an appropriate etching agent desired pattern is etched away from the first deposited layer[8]. Whereas, in lift-off a substrate is first coated with a photoresist consequently developed to form patterns (openings), through which the target material can reach the substrate. Then the target material is deposited to the whole surface, which covers the substrate as well as the undeveloped photoresist. Next, using a photoresist remover this undeveloped photoresist is washed away and the material above it is lifted-off together with this layer[5]. Fig 3.2 demonstrates the fabrication process of both of this processes, lift-off and wet etching.

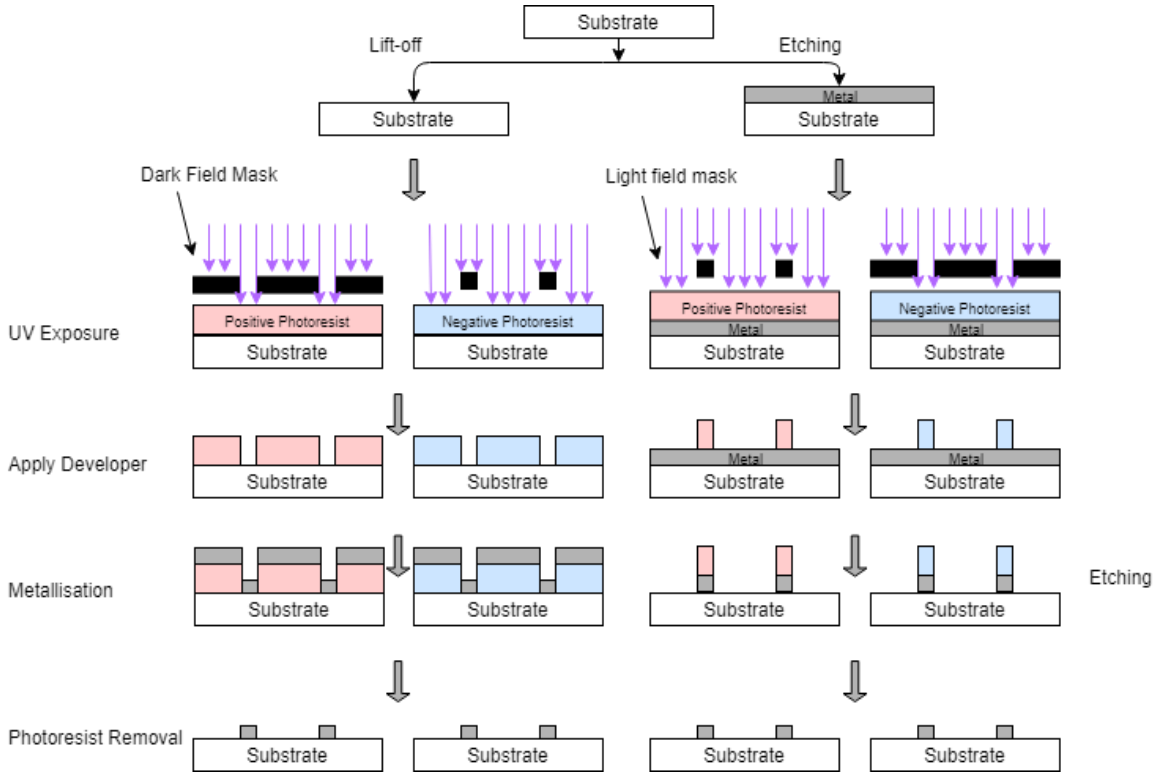

Figure 3.2. Combination of masks and lithography processes. A positive photoresist exposed through a dark field mask and a negative photoresist exposed through an opposite light field mask produce identical structures after lift-off and etching respectively.

Using different combination of masks and the lithography techniques it is possible to pattern exactly the same structures on a substrate, as shown in Fig 3.2. A positive photoresist ma-P 1210 and a negative photoresist SU-8 were available at UiT lab. SU-8 has better adhesion to PDMS compared to ma-P 1210 [11]. However, removing of SU-8 from PDMS surface is difficult once it is developed[5], which could lead to damaging the silver structures. Thus, positive photoresist along with the lift-off technique was chosen for fabrication.

This fabrication protocol was developed in three steps, each step involved parameter optimization:

- First lift-off was done on glass slides using a sample mask to test if lift-off works.
- Then lift-off was carried out on a glass slide coated with PDMS.
- Finally, lift-off was performed on a PDMS coated thermo-optics chip.

During the early phase of this thesis project thermo-optics mask and the chip were under fabrication in Barcelona. Silicon chips are both fragile and expensive compared to glass slides. In addition, there was no specific protocol available for the photoresist used in this thesis (positive photoresist ma-P1210). Therefore, to save time and study the initial challenges, lift-off process optimization was carried out on glass slides.

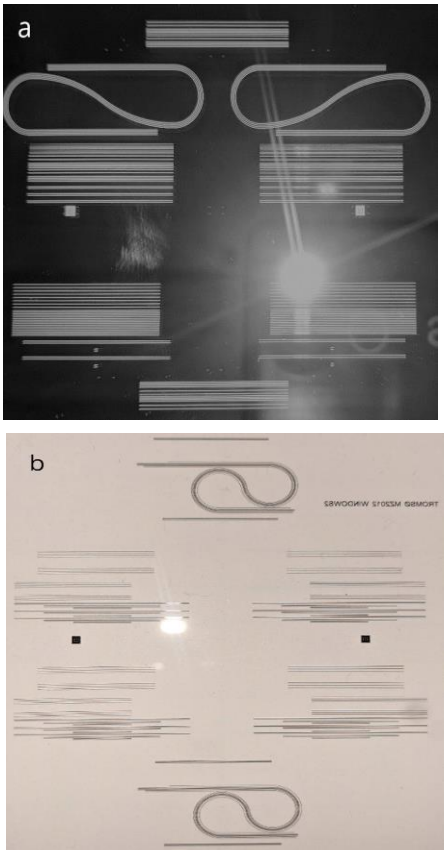

Figure 3.3. Examples of photolithography mask. (a) Dark field mask. Structures are transparent; the rest is opaque to light. (b) Light field mask. Opposite of dark field, light does not pass through the structures.

3.3.1 Materials and instruments

LOR, ma-P 1210 positive photoresist, mr-D 526/S developer and mr-Rem 700 remover were bought from Micro Resist Technology GmbH, Berlin, Germany. PDMS (SYLGARD™ 184 Silicone Elastomer Kit) and Hellmanex III were purchased from Sigma-Aldrich, Oslo, Norway. Microscope slides were ordered from VWR International AS, Oslo, Norway. WS-650MZ-23NPP/LITE spin coater, Laurell Technologies Corporation, North Wales, USA. MJB-4 Manual mask aligner, SÜSS MICROTEC SE, Garching, Germany. Plasma Cleaner, Harrick Plasma, Ithaca, NY, USA. P-6 Stylus Profiler, KLA-Tencor Corporation California, USA. Sputter coater 208HR, Cressington Scientific Instruments, Watford, UK. Hei-Tec magnetic stirrer, Heidolph Instruments GmbH, Schwabach, Germany. Vacuum drying chamber, BINDER GmbH, Tuttlingen, Germany. BX51 dark field microscope, Olympus Corporation, Japan.

3.3.2 Lift-off method on glass slides

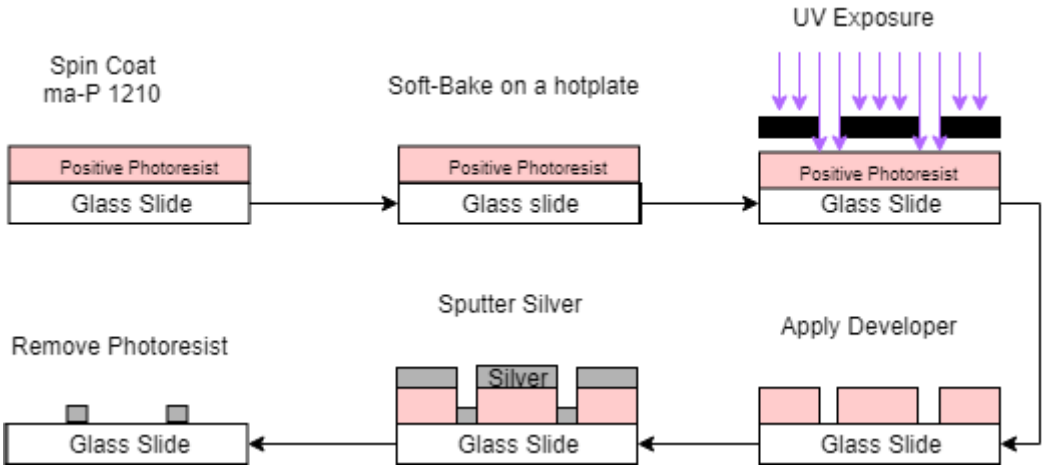

Figure 3.4. Lift-off process on a glass slide. Positive photoresist ma-P 1210 (micro resist technology GmbH) and its correspondent developer and remover is used for this process. Silver film is deposited by sputtering.

Entire fabrication process was carried out in a clean room under yellow light condition to avoid any unwanted exposure to the UV-sensitive photoresist (ma-P1210). Spin coating technique was used in Fig 3.4 and throughout the whole project to coat a thin uniform layer of this photoresist. To optimise the lift-off parameters 20 pre-cleaned microscope slides were prepared, each one covered with a thermal release tape on one side and numbered. This protected area was later used as a reference surface for thickness measurement. Photoresist was left in a glass beaker for about 10 minutes at room temperature to dissipate any dissolved air bubbles. Spin-coating ma-P 1210 for 30 seconds at 3000 rpm produces a film thickness of 1 μm [12]. Spin coater was pre-programmed to that configuration and a glass slide was secured to the spin chuck by turning on the vacuum. 400 μl photoresist was then dispensed on each slide using static dispense spin coating technique [13].

Ten slides were spin-coated at 3000 rpm for 30 seconds and ten slides at 2000 rpm yielding a film thickness of 1 μm and 1.5 μm respectively. Immediately after spin-coating these slides were baked on a hot plate according to the time and temperature specified in Fig 3.5.

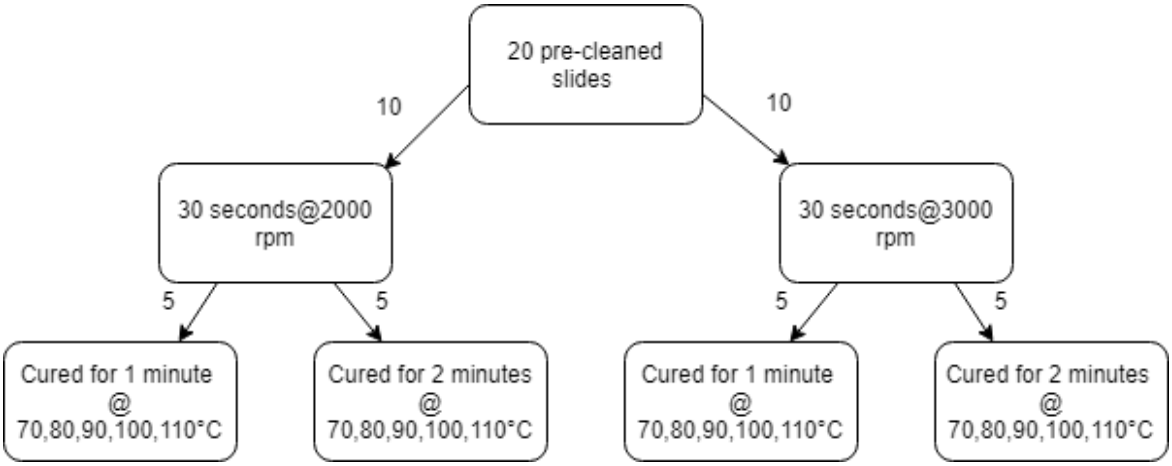

Figure 3.5. Optimization of lift-off process. Each of the 20 slides is numbered with a permanent ink. Ten slides are spin-coated at 3000 rpm for and ten slides at 2000 rpm 30 seconds yielding film thickness of 1µm and 1.5µm respectively. Five slides from each group backed on a hot plate for 1 minute and five for 2 minutes at temperatures from 70°C to 110° C followed by cooling in air for 1 minute.

Glass slides were then removed from the hotplate and cooled in air for 1 minute. Exposure Dose for 1 μm and 1.5 μm thick film of ma-P 1210 is 35 and 45 mJ/cm^2 (broadband exposure) respectively and a post exposure baking step is not necessary [12]. An UV-optometer supplied by the manufacturer of MJB-4 mask aligner was used to set the required exposure dose. Each glass slide was then exposed in soft contact exposure mode (a resolution of 2μm can be achieved in this mode[14]) using the dark field mask in Fig 3.3. After exposure, developed in mr-D 526 developer for about 30 seconds followed by gently rinsing with DI water and dried in N2. Each slide was then examined using a microscope with 10x magnification for any defects.

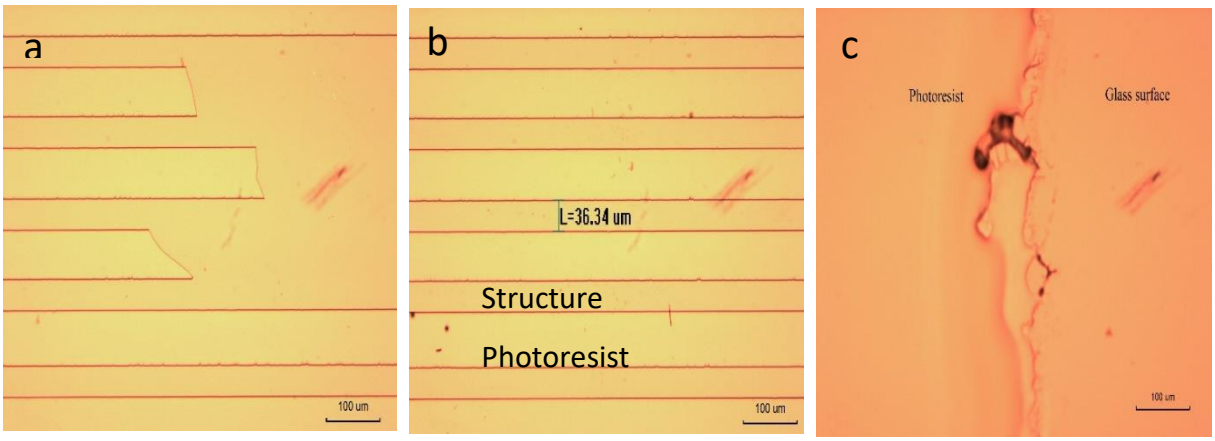

Figure 3.6. Effects of photoresist baking temperature and time (a) Temperature below 80°C, unexposed areas are also removed (b) Curing either 80°C or 90°C for 2 minutes produces identical structures as the mask. (c) Temperature above 90°C, and there is no pattern formation.

Curing at $80°C$ and $90°C$ for 2 minutes produced the finest patterns. For too low temperatures, adhesion to the glass substrate was so poor that unexposed photoresist was also removed, picture (a) in Fig 3.6. On the other hand, temperatures higher than 90° C were unable to produce any structures.

Best patterented slides (optimized parameters) were selected for the metallisation step and a sputter coater was used to deposit silver on those slides. Three different silver thickness were investigated for the lift-off $25nm, 50nm\ and\ 100nm$. The lift-off was done in mr-Rem 700 remover, silver structures were clearly visible after soaking in for 30 minutes. Glass slides were then taken out of the solvent, rinsed with DI water followed by drying in N2. Fine structures were formed on slides that were sputtered with $25\ nm$ of silver, Fig 3.7 (a) shows one of them, (b) and (c) shows the accuracy of the process.

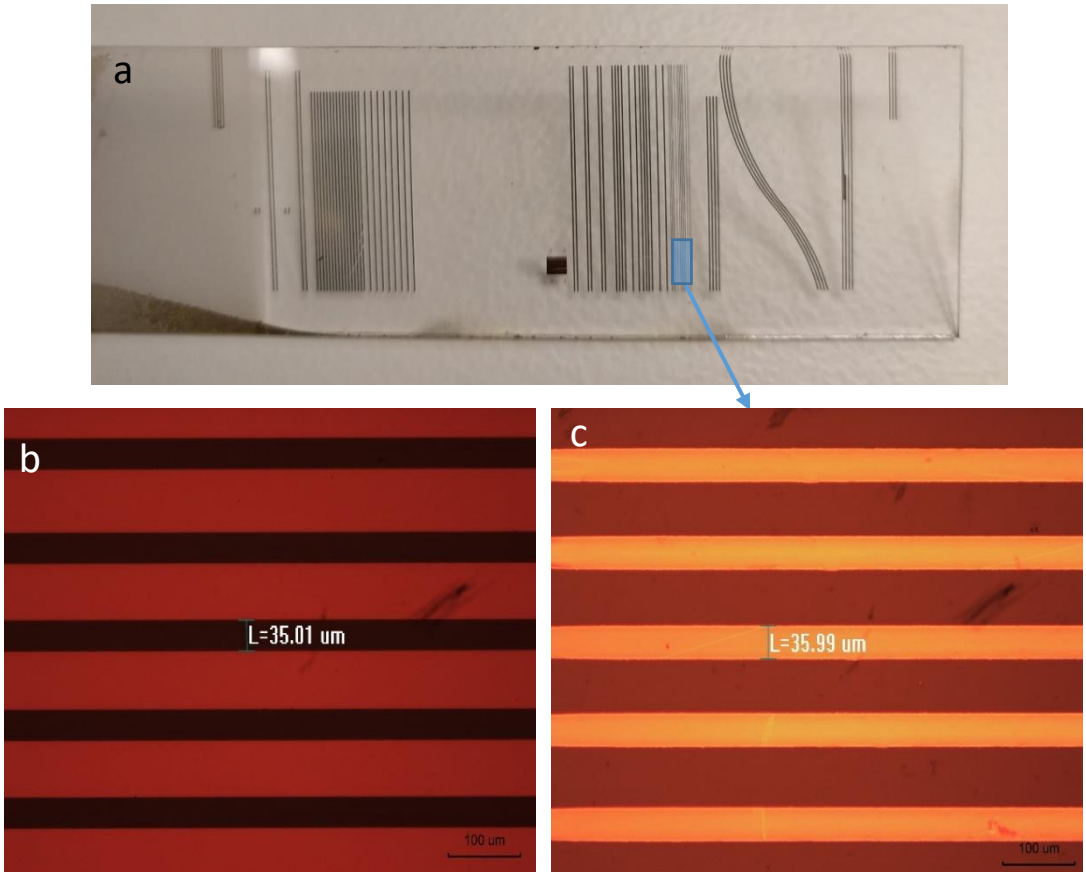

Figure 3.7. Pattern transfer on glass slides (a) Silver structures on glass after lift-off, silver thickness 25nm (b) and (c) 10x magnified area of the mask and the corresponding area on the fabricated structures.

3.3.3 Lift-off method on PDMS

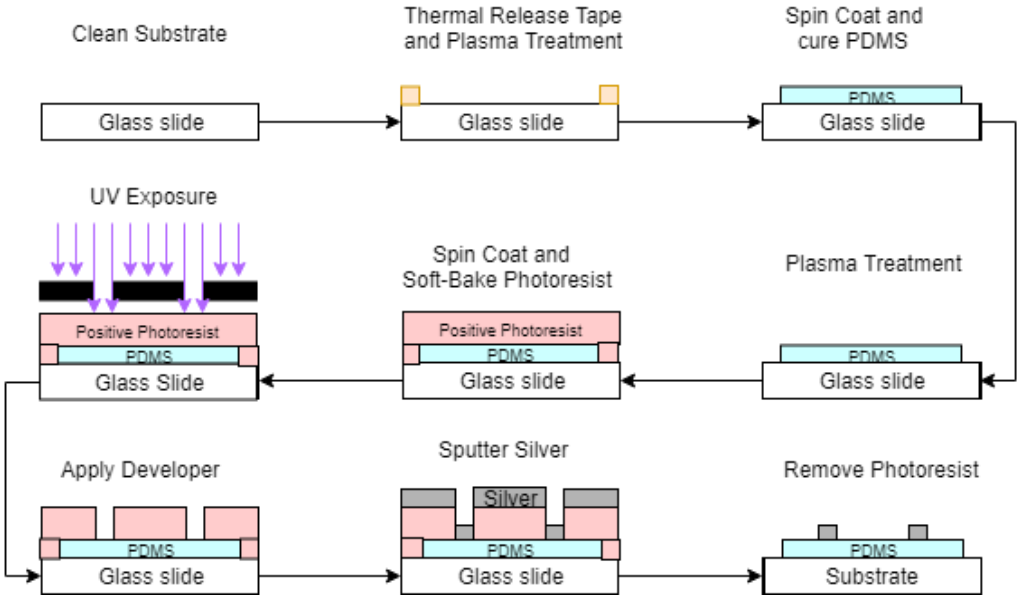

Figure 3.8. Lift-off process on glass slide coated with PDMS.

PDMS (SYLGARD™ 184 Silicone Elastomer Kit) was prepared by mixing the base and the curing agent at a weight ratio of 10:1. The solvent was degassed in a vacuum drying chamber for 15 minutes to dissipate air bubbles. Maximum bonding strength can be achieved between Glass-PDMS surface by treating glass slides in an ICP-RIE plasma [15]. In this experiment, glass slides were plasma treated in an ICP plasma for 20 seconds at a constant chamber pressure of 1000 mtorr. It is also recommended to use dynamic dispense spin coating technique for spin-speed above 1000 rpm[16]. However, with this technique it was not possible to produce a layer of uniform thickness due to the high viscosity (3500cP) of PDMS[17]. So, the dispense technique was slightly modified to get the best result. 500 μl of PDMS was dispensed on a plasma treated glass sided while the spin-coater was stand still, then it spun for 10 seconds at 500 rpm followed by 5 minutes spin at a speed specified in the following graph:-

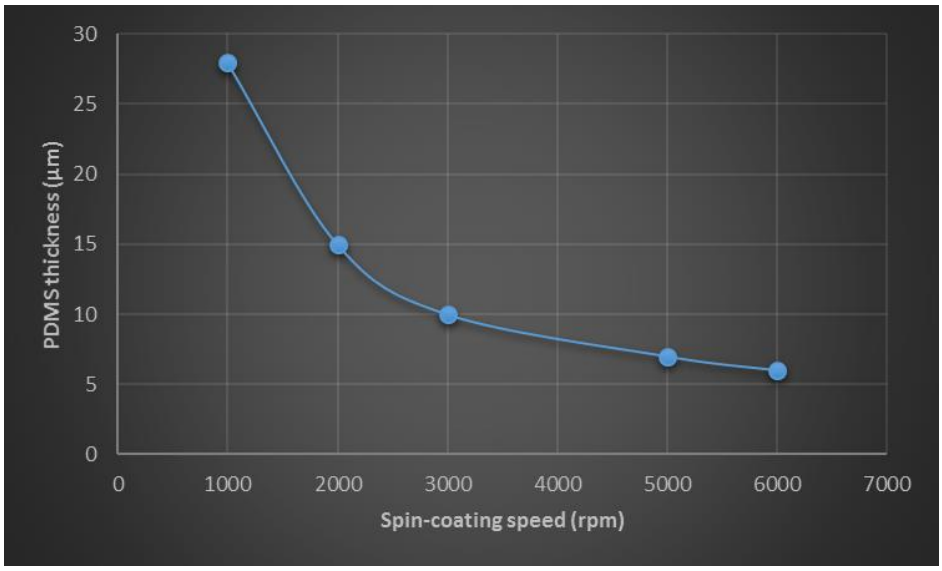

Figure 3.9. PDMS thickness a function of spin speed for a rotation time of 5 min. PDMS (SYLGARD™ 184 Silicone Elastomer Kit) was prepared by mixing base and curing agent at a weight ratio of 10:1. Degassed for 15 minutes in a vacuum drying chamber to dissipate any air bubbles.

After spin coating, PDMS was cured on a hotplate for 20 minutes at 125°C, cooled down to room temperature by turning off the heater. Then the intention was to follow the same protocol on PDMS surface, which was developed for glass in section 4.2.2. However, it did not work due to the poor adhesion between PDMS and photoresist. Wettability of a material is characterised by its contact angle. Lower contact angle corresponds to hydrophilic materials and higher contact angle means the material is hydrophobic. The contact angle of PDMS is very high 109° compared to 20 ° of glass [15], meaning PDMS surface is highly hydrophobic. Any attempt to coat photoresist on PDMS failed, as can be seen in Fig 4.7 (a). Then the following steps were performed to overcome this problem:-

- PDMS surface was treated with UV-exposure of varying doses, none of them worked.
- PDMS was treated in plasma for 20 seconds at 1000 mtorr. After plasma treatment, PDMS-photoresist bonding worked Fig 4.7 (b), but the lift-off did not work because the bonding strength was too strong, Fig 4.7 (c) shows the result.
- A thin layer of LOR ($1\mu m$) was used as a sacrificial layer between PDMS and photoresist to eliminate the need of plasma treatment. PDMS-LOR-Photoresist bonding worked, but formed severe crack during soft-baking.
- Consequently, plasma treatment time had to be optimised. Different plasma treatment time between 1 and 20 seconds were tested, 5 seconds at 1000 mtorr plasma treatment produced the expected result in Fig 4.7(d).

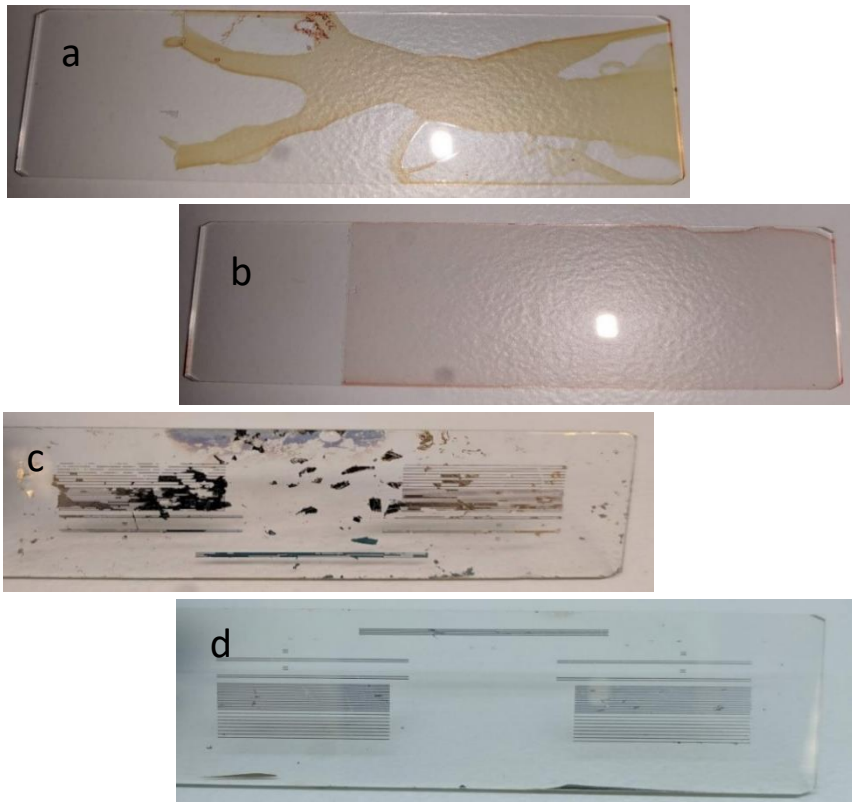

Figure 3.10. Effects of plasma treatment. (a) ma-P 1210 photoresist is optimized for application on rigid substrates only, thus adhesion is very poor when applied to PDMS surface (b) Adhesion between PDMS and photoresist gets better with seconds plasma treatment (c) Bonding between photoresist and PDMS is too strong for 20 seconds plasma, lift-off does not work. (d) Plasma treating PDMS surface for 5 seconds produces expected result.

3.3.4 Lift-off on thermo-optics chip

Exact same protocol was followed for the thermo-optic chip as the one developed in previous section for PDMS except for the chip preparation and mask alignment steps.

Chip preparation

Six chips were fabricated in one Si wafer and each one was diced after fabrication. Polishing with ultra-fine sand paper ($10\mu m \; and \; 5\mu m$) was required in order to have better laser coupling. Polished chip was cleaned in acetone for 20 seconds, rinsed with an IPA stream then DI water followed by drying in N2. Then the chip was socked in 1% Hellmanex III solution and heated to 70° for 10 minutes. After that, it was rinsed in DI water for 30 seconds to wash away any remaining solvent and dried in N2. Before spin coating PDMS, uncladded imaging area and the coupling ends were protected using a thermal release tape, as shown Fig 4.9.

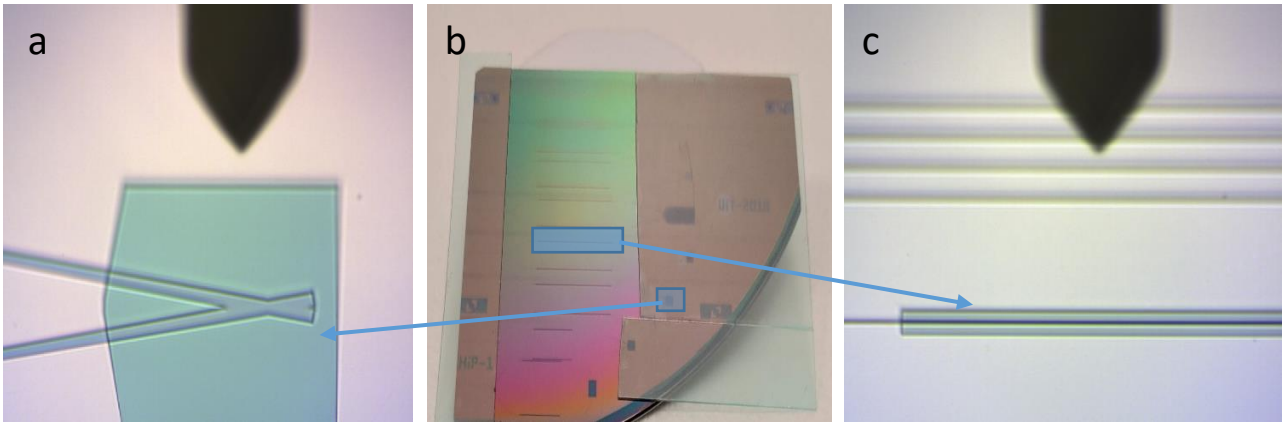

Figure 3.11. Uncladded area on the chip. (a) Adiabatically tapered waveguide in the imaging area, covered with thermal release tape before spin-coating PDMS (b) the thermo-optic chip (c) Opening area on the interferometer's waveguide arm. Each arm has an identical opening; PDMS gets in contact with both waveguides after spin coating. Silver micro heater is deposited on one of the arm.

Mask Alignment

Cured photoresist film is brittle, slightest strain causes crack to form on the surface. Therefore, the soft contact exposure mode was chosen to avoid direct contact with the mask. In addition, alignment tolerance was quite high as the silver structures were 30 times wider than the waveguide.

Exposure dose was measured using the test exposure mode and the UV-optometer. Contact gap between the mask and the chip was adjusted using the WEC settings knob. Each chip was designed with four diagonal alignment marks (Fig 4.10 (a)) one on each corner and the mask had the same counterpart markings. Alignment was done using the $x-axis, y-axis$ and $\theta-axis$ knobs on the mask aligner. After alignment, the chip was exposed with the pre-programmed dose and the rest of the lift-off process was carried out on that chip.

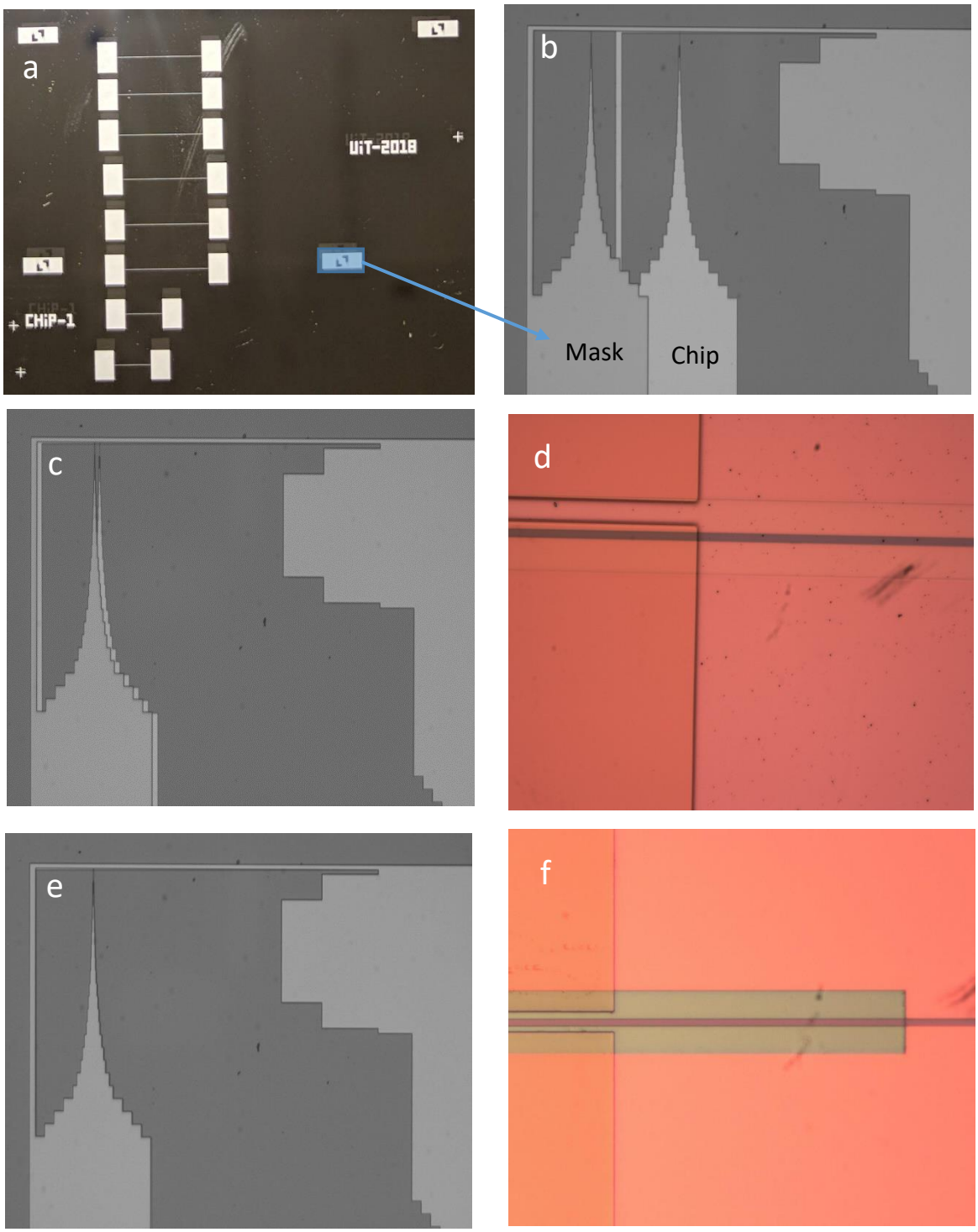

Figure 3.12. Process of mask alignment. (a) Thermo-optics mask with alignment markings on each corner (b) Same alignment mark on the chip, diagonal markings are used for the alignment (c) and (d) are the effects of misalignment (e) and (f) are properly aligned mask.

PDMS has a CTE (Coefficient of Thermal Expansion) of $340\ ppm/°C$ [17] and the photoresist is typically below $100\ ppm/°C$. Most of this photoresist are optimized for hard substrate like glass or silica which has a lower CTE. During photoresist baking process, PDMS and photoresist expands and shrinks at a different rate due to this CTE mismatch. As a result, severe microscopic crack forms on the photoresist surface (Fig 4.11 (a)) and also appears on the patterned silver lines (Fig 4.11 (b)). This problem was solved by reducing the thermal stress during softbake.

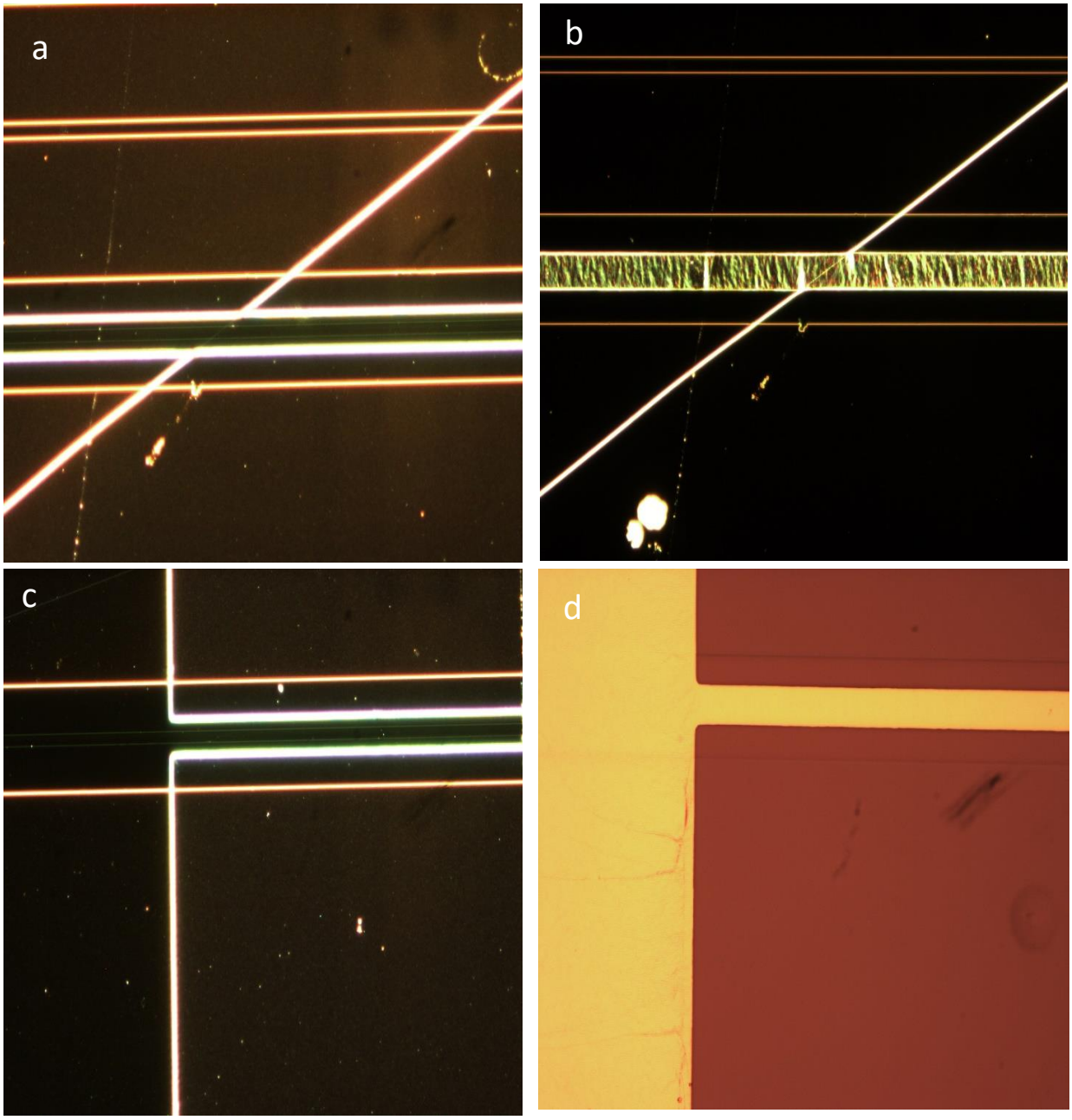

Figure 3.13. Dark field images of microscopic crack on the chip, (a) Cracks are formed on photoresist due to higher thermal expansion rate of PDMS (b) This crack makes the thermo-optics unusable. (c) and (d) Cracks are minimised by ramping temperature up from room temperature to 80°C over one minute, held for 2 minutes followed by cooling down to room temperature by turning off the hotplate.

3.3.5 Summary of the lift-off protocol

- Polish, clean and cover the chip with thermal release tape where PDMS is not needed
- Treat in ICP plasma for 20 seconds at a constant chamber pressure of 1000 mtorr
- Spin-coat PDMS for 10 seconds @ 500 rpm & 5 minutes @ 6000 rpm to produce $6\ \mu m$ thick film
- Bake on a hotplate for 20 minutes @ $150\ ^\circ C$, turn off the hotplate, let it cool to room temperature
- Plasma treatment for 5 seconds at 1000 mtorr constant chamber pressure
- Immediately apply photoresist (ma-P 1210) and spin @ 2000 rpm for 30 seconds
- Place on a hotplate and ramp the temperature up from room temperature to $80\ ^\circ C$ over one minute, bake for 2 minutes, cool down to room temperature by turning off the heater
- Expose with the required does (45 mJ/cm^2 for 1.5 µm film) using the dark field mask
- Develop in mr-D 526/S developer for about 30 seconds, until the patterns are visible
- Wash the surface with DI water for 30 seconds and dry in N2
- Inspect the chip under a microscope for defects, apply silver film using a sputter coater
- Soak in mr-Rem 700 remover for 30 minutes, followed by cleaning with DI water and drying in N2

Following these steps will produce a complete thermo-optics chip as shown in Fig 4.11 (b).

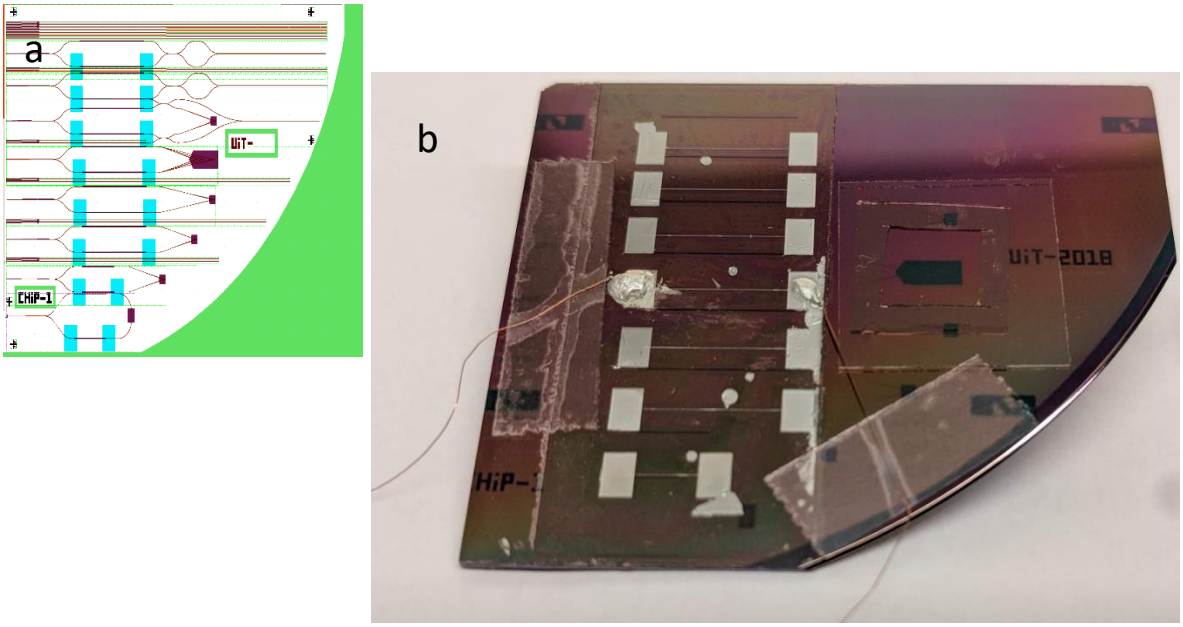

Figure 3.14. (a) Design of the thermo-optic chip. (b) Complete chip with the thermo-optics and connected to 80µm insulated copper wires

4 Preliminary data on phase measurements

In this chapter, preliminary results from the phase measurements are discussed. In section 4.2, we presented analytical and experimental results of interference fringe spacing measurements using fluorescent dye and in section 4.3 phase shift measurements using fluorescent beads are presented.

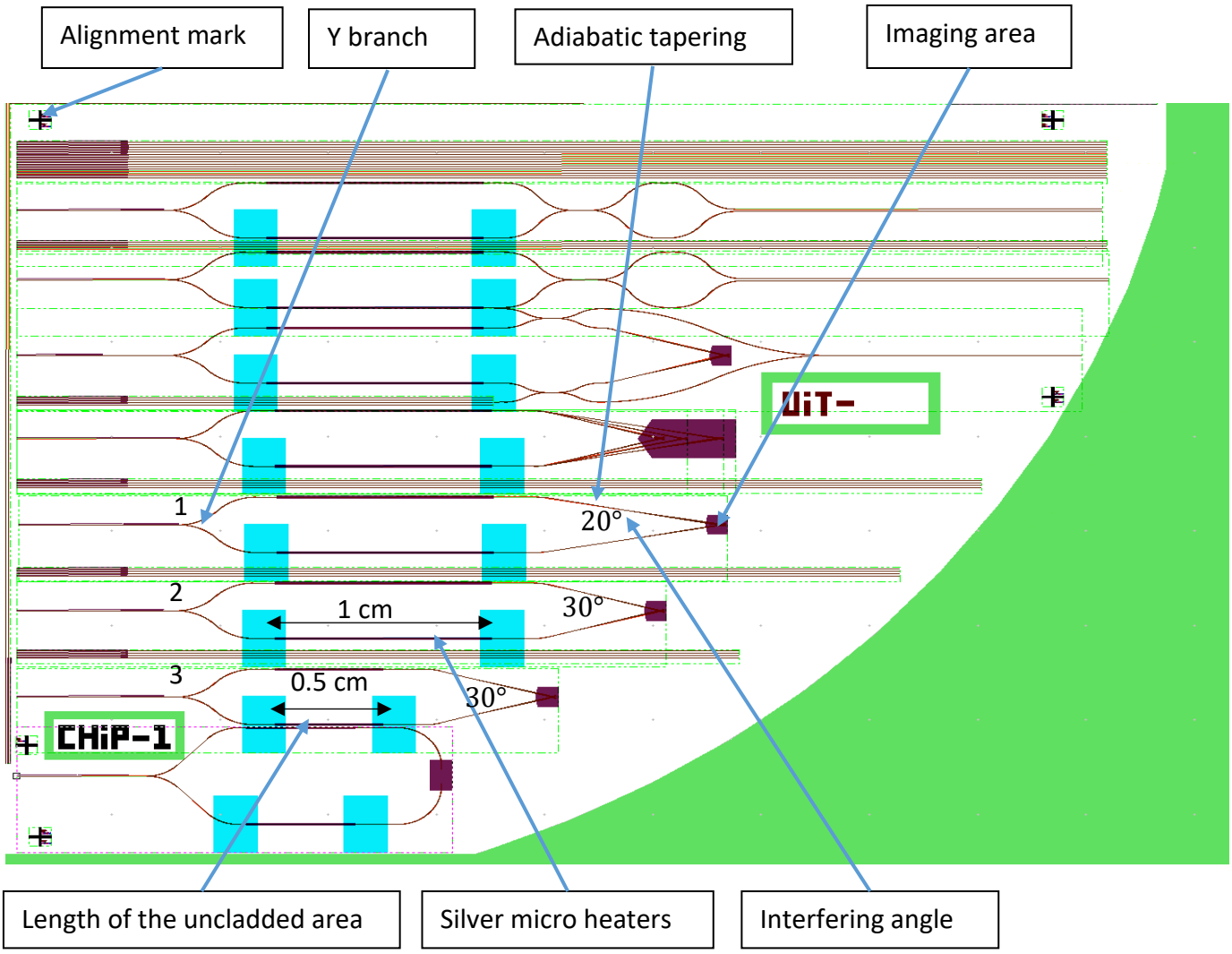

Figure 4.1. Design of the thermo-optic chip, designed in CleWin5. Laser is coupled into the Y branch, divided 50/50 in each waveguide arm and meets at the imaging area through adiabatic tapering. Each arm has an open (uncladded) area of equal length covered with PDMS and one of them has a heating element on top.

4.1 Experimental methods

4.1.1 Materials and instruments

CellMask Deep Red (CMDR), CellMask Orange (CMO) and TetraSpeck Microspheres (#T7279), 0.1 µm, fluorescent (blue/green/orange/dark red) were ordered from Thermo Fisher Scientific, Waltham, USA. 22mm x 22mm Corning cover glasses were bought from Sigma-Aldrich Norway AS, Oslo, Norway. Toptica iChrome MLE Laser with 4 wavelengths $(405nm, 488nm, 561nm, 640nm)$, TOPTICA Photonics AG, Munich, Germany. IDS UI-3060CP Camera, IDS Imaging Development Systems GmbH, Obersulm, Germany. Custom built Olympus microscope with 10x, 20x and 60x water immersion lenses. Agilent E3631A 80W Triple Output Power Supply, Keysight Technologies, California, USA.

4.2 Interference fringe spacing measurements using fluorescent dye

Interference patterns are not visible on scattered images, as can be seen from Fig 4.3 (b). Scatterers on chip emit light at same wavelength as the excitation beam. The scattering happens due to any hot-spots or impurities on top of waveguide surface. To be able to capture the interference patterns, a fluorophore dye is used which has an emission wavelength different from the excitation wavelength. Then, by using an appropriate filter it is possible to block the scattered light from the fluorescence signal. CellMask are a type of dye used in fluorescence imaging to stain cell plasma membranes. CellMask deep red is excited by $640\ nm$ and has emission maxima at $666\ nm$. For CellMask orange its $561nm$ and $567nm$, respectively.

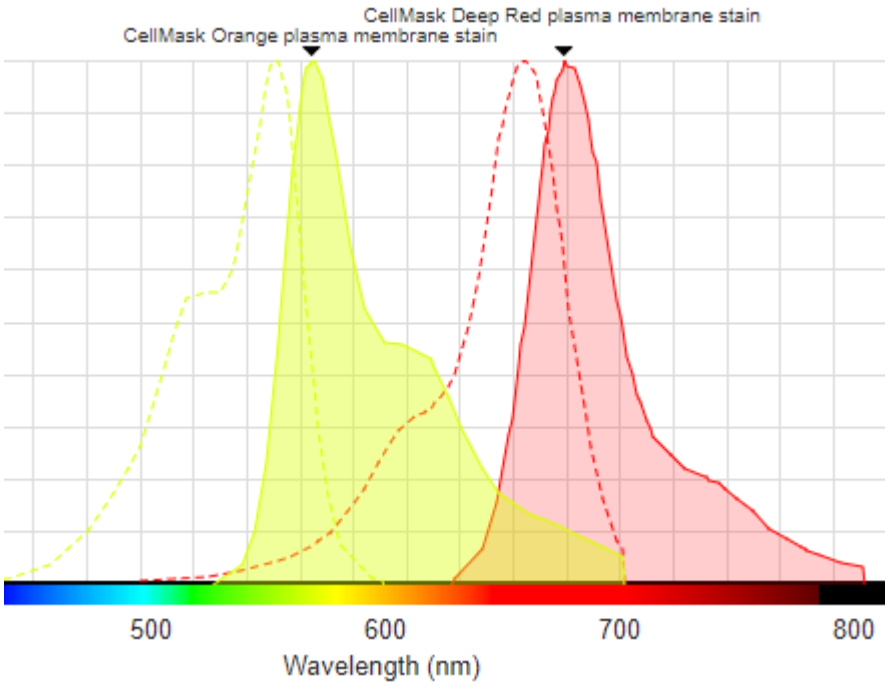

Figure 4.2. Excitation and emission spectra of CellMask plasma stain[1].

Chip preparation with fluorescent dye

For both dyes (CMDR and CMO), a dilution of 1:1000 was prepared by mixing the stock solution with DI water. Imaging area of the chip was pre-cleaned using acetone and water and dried in N2. A $150\ \mu m$ thick PDMS chamber was cut out to border the imaging area, so that the solution stays in place during imaging. About $20\ to\ 30\ \mu l$ (depending on the size of the PDMS chamber) of this solution was added to the imaging area and kept under a dark shade for 10 minutes. After 10 minutes, the imaging area was washed with DI water twice. Then, a droplet of water was placed on the imaging area and a cover slip above it. Finally, by gently pressing the cover with a pair of plastic tweezers the whole area was sealed.

Fig 4.3(c) shows the result of filtering out the scattered light. An appropriate filter is used according to the wavelength to filter out the excitation and the scattered light, letting only the light from the dye to be captured by the camera. It is evident form Fig. 4.3 (c) that the field is not very uniform and there are some light strips which is possibly due to shadowing effect or mode beating, although the waveguide was designed for single mode conditions.

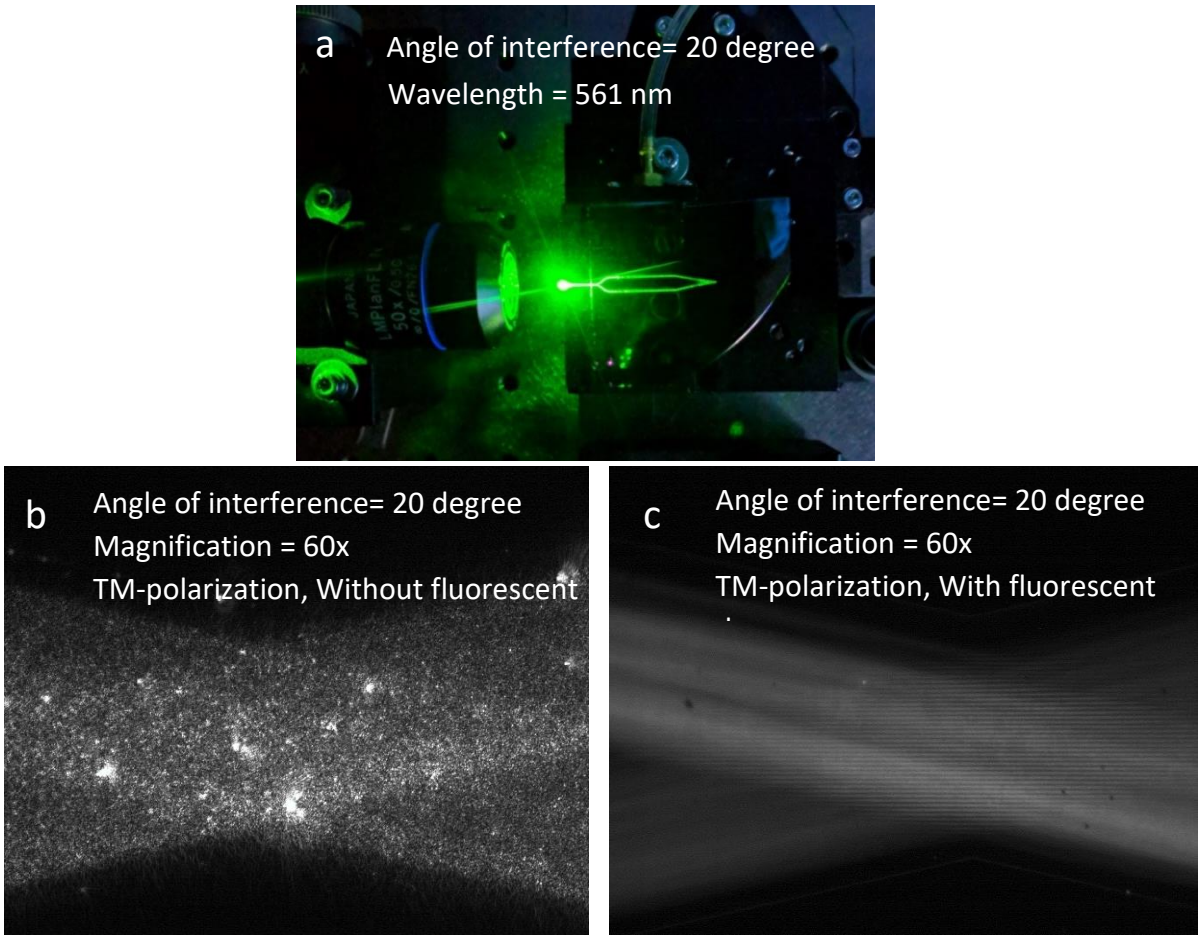

Figure 4.3. (a) Effects of scattering (b) Interference patterns are not visible due to scatterers (c) Interference patterns made visible by using fluorescent dye (which emits light at a different wavelength than the illumination light) and an appropriate filter is used to filter out the illumination and scattered light.

Magnification of an objective lens is its ability to make smaller objects appear larger while, resolution is the ability to distinguish two objects from one another. Resolution of a microscope is limited by the abbe diffraction limit, $d = \frac{\lambda}{2NA}$ [18]. For air the theoretical maximum NA can be as large as 1. For other immersion medium like oil or water it can have a value more than 1. Table 4.1 shows the maximum achievable resolution according to NA, which helps to decide what objective lens to choose.

Objective lens		Resolution (nm) @ 640 nm	Resolution (nm) @ 561 nm
Magnification	NA		
60X: oil immersion	1.3	246	215
60 X: water immersion	1.2	266	233
20X	0.45	711	623

Table 4.1. Resolution as a function of objective lens NA and wavelength ($d = \frac{\lambda}{2NA}$).

The thermo-optics chip was designed to study the interference pattern and phase shifting property at different interfering angles ($20°\ and\ 30\ °$). Fig 4.4 (a) and (b) are the captured interference patterns of $20°\ and\ 30°$ angle, (c) and (d) are the close up view, respectively. $20\ °$ Interference patterns are seen (c), visibly and also with FFT Fig 4.4 (e). According to the analytical result, for $640\ nm, TM$ and $30°$ interfering angle, fringe spacing is $0.78\mu m$ (Table 5.3). These fringes should also be visible using a $20x, 0.45NA$ objective lens, which has a resolution of $0.71\mu m$ at that wavelength. However, this was not observed, FFT of the image shows no peak Fig 4.4 (f). It should be emphasised that the Abbe's diffraction limit gives theoretical limit of the resolution using the objective lens when operated in the ideal situation with an ideal microscope. However, in most practical microscope the resolution is slightly worse than the Abbe's diffraction limit. This is due to under-filling of the aperture of the objective lens, and other miss-alignment of the optical system. So, to overcome this problem, from this point forward all the measurements are taken using 60x, 1.2NA.

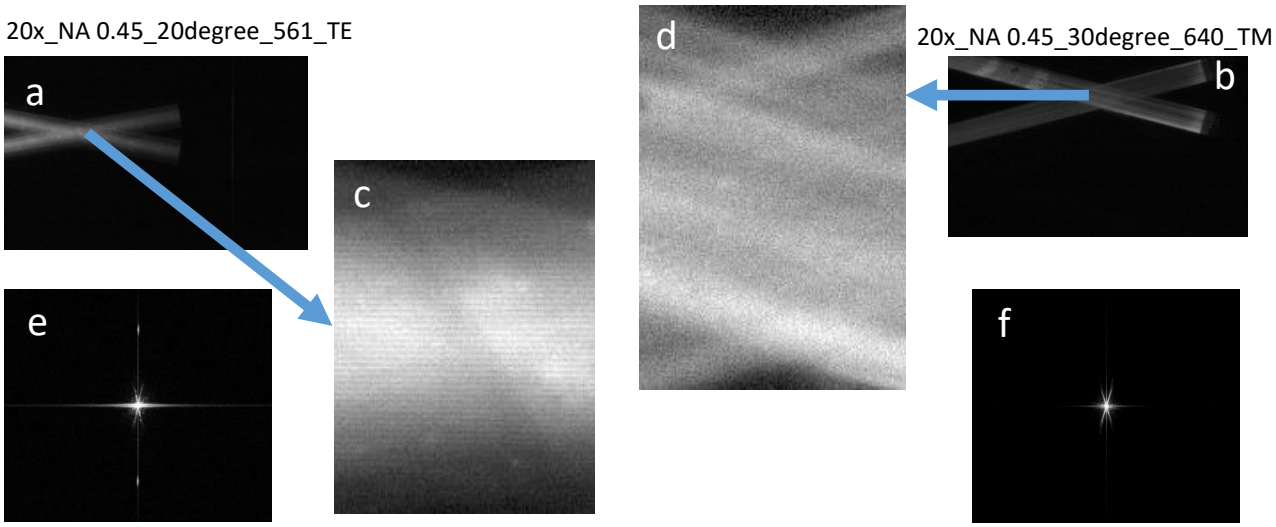

Figure 4.4. Abbe diffraction limit of a 20x, 0.45 NA objective lens. (a) and (b) are the interference patterns from 20-degre and 30-degree interference angles, respectively. (c) and (d) are the zoomed in views. (e) and (f) shows the FFT of those images. 30-degree interference patterns are limited by the abbe diffraction while 20-dregee is visible.

Specifications	IDS_uEye
Effective number of pixels (h x v)	1936 x 1216
Optical area (mm^2)	11.345 x 7.126
Optical area with 60 x magnification (μm^2)	189 x 119
Pixel size (µm)	5.86
Pixel size with 60 x magnification (nm)	98
Pixel size with 20 x magnification (nm)	293

Table 4.2. Pixel size conversion chart for IDS_uEye UI-3060CP Camera

For a microscope camera, with increasing magnification, effective size of the camera pixel decreases. In table 4.2, each pixel size of IDS_uEye camera is converted to the effective pixel size according to the magnification of the objective lens. The camera can capture a total area of $189\mu m \times 119\ \mu m$ using a 60x objective lens, which was sufficient for our experiment. These waveguides are designed to maintain single mode condition at $561nm\ and\ 640nm$, so there is only one strong interference in the centre region where the two mode profiles meet. Inference fringe spacing is analysed using Fiji[19] image processing software. A line profile (Fig 4.5) is plotted across the centre of the interference region and the total number of pixels are converted to length by multiplying with $98nm$ (effective pixel size with 60x magnification). Each peak and trough in the line profile represents a constructive and a destructive interference, respectively. Note that the interference pattern is recorded using a florescent dye, the intensity also depends on how well the dye is distributed across the imaging area. Thus, our calculation is based on the average spacing between 5 to 6 consecutive peaks, which produces better accuracy in measurements.

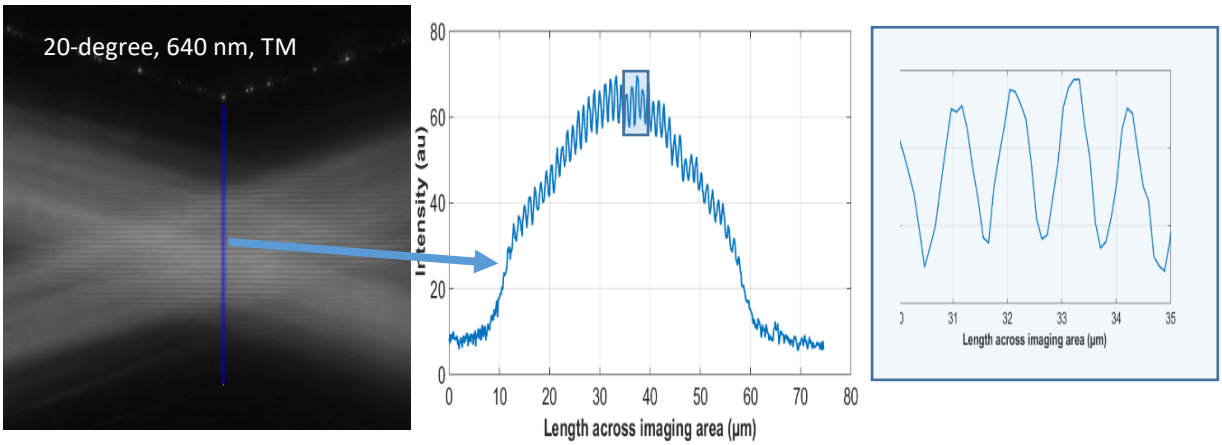

Figure 4.5. Methods for calculating fringe spacing. Line profile across the interference region is converted to length in µm to calculate the spacing between two peaks

$$Interference\ fringe\ spacing, d_f = \frac{\lambda}{2 * N_{eff} * \sin\left(\frac{\alpha}{2}\right)} \ldots\ldots\ldots\ldots\ldots\ldots\ldots\ldots\ldots\ldots (1)$$

$$N_{eff} = Effective\ refractive\ index\ of\ the\ imaging\ area$$

$$\alpha = angle\ between\ the\ interfering\ waveguides$$

60x Water immersion lens is used to capture the interference patterns. As the name suggests, NA of this lens is only corrected for water. SiO2 is the top and bottom cladding material for this chip except for the imaging area. In the imaging area bottom cladding is still SiO2 but there is no top cladding, so that any immersion medium can be used as a top cladding. Refractive index of water is $n = 1.33$ and for SiO2 $n = 1.45$. If this imaging area had a top cladding of SiO2, the refractive index mismatch between the immersion medium and top cladding would result in imaging aberrations. N_{eff} For TE is 1.72 and for TM polarization its 1.59, considering water as the top cladding *(the simulation was done by Dr*. Firehun Tsige Dullo using Fimmwave). *They are* different for TE and TM mode due to the boundary condition of the waveguide (rib waveguide geometry). It is clearly evident from equation (1) that the interference fringe spacing is a function of the wavelength, polarization and the angle of interference. Analytical and the experimental results are shown in Table 4.3.

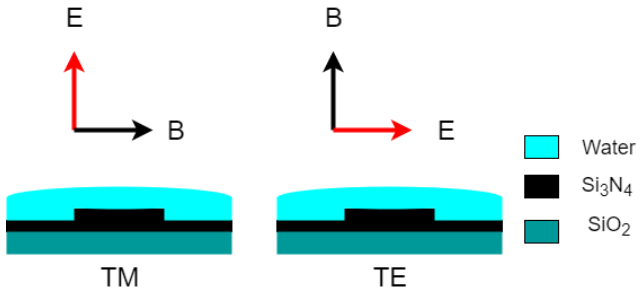

Figure 4.6. Electric field orientation in TM vs TE mode.

- N_{eff} for TM mode is smaller than TE mode, so for the same wavelength TE mode produces narrower interference fringes.
- For the same polarization, shorter wavelength produces narrower fringes.
- And for the same polarization and wavelength, larger interference angle produces narrower fringes.

Wavelength (nm)	Angle between the interfering waveguides (degree)	Spacing between fringes (µm)			
		Analytical		Experimental	
		TE	TM	TE	TM
640	20	1.07	1.16	1.07	1.18
	30	0.72	0.78	0.72	0.78
561	20	0.92	0.99	0.88	0.98
	30	0.62	0.66	0.59	0.68

Table 4.3. Spacing of fringes as a function of angle, wavelength and polarization, numbers are rounded up to the nearest digit.

4.3 Thermo-optical phase shift measurements using fluorescent beads

TetraSpeck beads used for this experiment are 100nm in diameter and can be excited by 4 different wavelengths, excitation/emission wavelengths are $360/430\,nm\,(blue)$, $505/515\,nm\,(green)$, $560/580\,nm\,(orange)$ and $660/680\,nm\,(dark\,red)$ [20]. These fluorescent beads are better than using fluorescent dyes Using this florescent beads for phase measurement has some advantages over fluorescent dyes for the phase measurement as, beads are more stable, have better visibility, can be easily prepared as sparse samples and image processing with Fiji is much easier.

Chip preparation using beads

Stock solution of TetraSpeck Microspheres was placed in a centrifuge for about 20 seconds at 4500 rpm. A PDMS chamber was used to make a border around the imaging area. Then, $1\,\mu l$ of the stock solution was added to the pre-cleaned imaging area and dried under a dark shade for 10 minutes. A droplet of water was then added to the imaging area and using a coverslip the whole area was sealed.

Methods for capturing and analysing beads data

This image capturing and processing technique is used for the next six experiments. In each case, a power supply is connected to one of the phase modulators and an IDS camera is attached to a $60x, 1.2NA$ objective lens. A python[21] programme *(written by fellow PhD student Øystein Ivar Helle)* controls the power supply and capture images at the same time. It also records supply voltage to the phase modulator, current and image capturing time. Camera requires around 100ms exposure time to capture sufficient florescence signal from fluorescent beads and the power supply takes almost 700ms to response to this Python command. So, our temporal resolution is limited to around 800 milliseconds.

For each experiment a sequence of picture is captured. Then, an image stack is produced from this image sequence using Fiji [19]. An image stack is a combined file of all the images stacked from first image to the last. Then the intensity is adjusted using $Auto$ function under brightness and contrast settings. From this image stack (Fig 4.7 (a)) one small sparse bead is selected to plot its z-profile. The z-profile in (Fig 4.7(b)) represents beads behaviour in time.

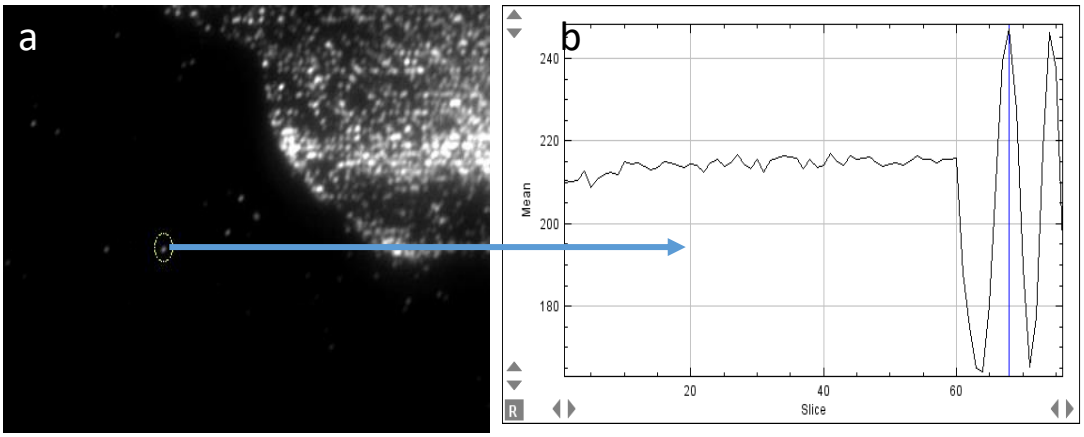

Figure 4.7. Method of processing beads image. (a) An image stack is formed from 75 images (b) is a z-profile plot of a bead selected from the left picture, plot shows intensity variation in y axis and the total number of images in x, from 0 to 60 images intensity fluctuation is very slow compared to 60 to 75

4.3.1 Cross-heating between the interferometer arms

This experiment shows the effect of heat transfer from one arm of the phase modulator to the other, which helps to determine the maximum duration for recording a phase change event.

A computer-controlled power supply (as discussed in the previous section) was connected to the *0.5 cm* length silver micro-heater and the input waveguide was coupled with a 640nm, TM polarized laser with 10 mW power.

Fig 4.8 shows the experimental result that demonstrates cross-heating problem. 120 images were captured for one plot. Each graph in Fig 4.8 is a z-profile plot of a single bead selected from an image stack. Results are plotted against time. In Fig 4.8 (a) from 0 to 15 seconds there is no power supply, then the voltage is raised from 0 to 2 volts and kept constant for 95 seconds. For (b) and (c) same procedure but instead 0 to 3 volts and 0 to 4 volts, respectively. Orange lines indicate voltage and the blue lines indicate beads intensity change over time. Ehen the input power is switched on, the silver micro-heater is heated up, and this heat changes the phase of one of the waveguide arm causing the change in the intensity of the beads. Phase change is described elaborately in later sections, for now we will try to understand the effects of cross-heating.

In the vertical direction, from the silver micro-heater to the waveguide the distance is $8\mu m$ (thickness of PDMS). And in the lateral direction from silver micro-heater to the other interferometer arm 3.5mm. When the temperature difference between two arms is zero (0 to 15 seconds), there is no phase change. As heat starts to change (rise in our case) in one arm as compared to the other arm, the phase follows this change (seen by the blue line following the orange line in the plot). PDMS also transfers heat in the lateral direction towards the other arm and at some point heat between the two arms equalize and the phase returns to the initial state (i.e. no phase change). For the first two plot, *(2 volts and 3 volts)* this effect is not so significant, since there is less heat to transfer.

Nevertheless, at 4 volts heat transfer between the arms is so fast that after about 15 seconds phase decays to its initial state. This may not cause a problem for actual SIM imaging because SIM only needs 3 phase steps few hundred milliseconds apart, but for our phase experiments, the voltage steps should be adjusted in such a way that the total measurement is done in less than 15 seconds when working with 4 volts or more.

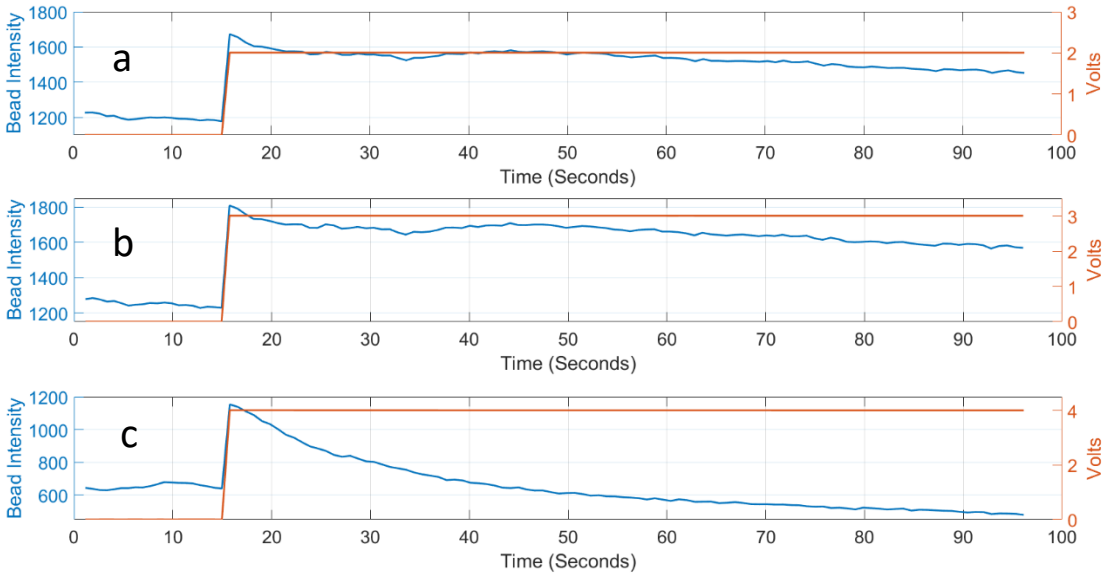

Figure 4.8. Cross-heating between the interferometer arms. As the voltage increases the increased temperature from one arm starts to heat the other interferometer arm. In the third graph, at 4 volt cross-heating between the two arms is so fast that after about 20 seconds temperature in both arm equalizes and phase (bead intensity) returns to the initial state.

4.3.2 Phase Repeatability

For SIM imaging, illumination pattern from a thermo-optic phase modulator chip has to meet some criteria:

1. High visibility, i.e. the ratio between the minimum and the maximum phase intensity needs be large enough so that it is distinguishable
2. Phase change should be repeatable over time
3. Phase response time needs to be small
4. The power it takes to change the phase should be reasonable

From this experiment we will observe the phase behaviour in first three aspects, power will be discussed in later sections.

Phase modulator with 0.5cm sensing length (Fig 4.1 (3)) was tested for phase repeatability. This experiment was done using 640nm, TM polarized laser at 10 mW. For the fringe spacing measurement with fluorescent dye, only 2-3 mW power was used. However, Fluorescent beads are more stable than fluorescent dye so it does not bleach out quickly even with more power.

Fig 4.9 shows the intensity change of a single bead plotted against time. 350 images are recorded in real time, each event takes $\approx 800\, milliseconds (total\ \ time, 350 \times 0.8 = 280\, Seconds)$. For each of the first 50 images python program writes 0 (zero) volt to the power supply and captures one image after each command, tiny fluctuations in the graph shows the effect of background noise (i.e. environmental temperature change, noise from the power supply). Then the voltage is increased from 0 to 1, because it has been observed from previous experiments that the phase starts to change around 1 volt, and also to keep the total

time of voltage stepping below 15 seconds (as discussed in the cross-heating section). Then from 1 to 5.5 volts, voltage is increased in steps of 0.3V ($total\ time\ from\ 0\ to\ 5.5\ V \approx 17 steps \times 0.8\ seconds\ = 13.6\ seconds$), black markers in the plot indicates these voltage steps. After 5.5 volt the power supply returns to 0 volt again and the program keeps recording pictures for another 50 steps. The whole process repeats three times.

Each waveguide arm is covered with PDMS, where evanescent field penetrates. With each successive voltage step, silver micro heater takes current and heats up the PDMS layer below it, while temperature of the other arm remain unchanged. This change in temperature causes refractive index of PDMS to change in one arm. Refractive index is a function of temperature as shown in Eq.2 and as temperature is changed the refractive index changes. It is the thermo-optical coefficient of the material.

This phase change is observed as an intensity change of a bead. This concept may be hard to grasp at first, but the bead can be thought of as a tennis ball floating on water wave. Beads intensity reaches its minimum value when it is between two waves and maximum when on top of a wave peak.

From Fig 4.9 it is obvious that the phase starts to change as soon as the voltage jumps from 0 to 1 volt (i.e. phase response is very fast possibly in the order of milliseconds). Ratio between the maximum and the minimum intensity is high and the phase change behaves in exactly same way for the repeated steps (a,b,c). However, in each case it takes quite some time for the phase to decay even after switching off the power supply. A possible explanation for this could be that, the chip and its surroundings also get heated to a certain temperature along with the PDMS, thus the heat dissipation takes longer.

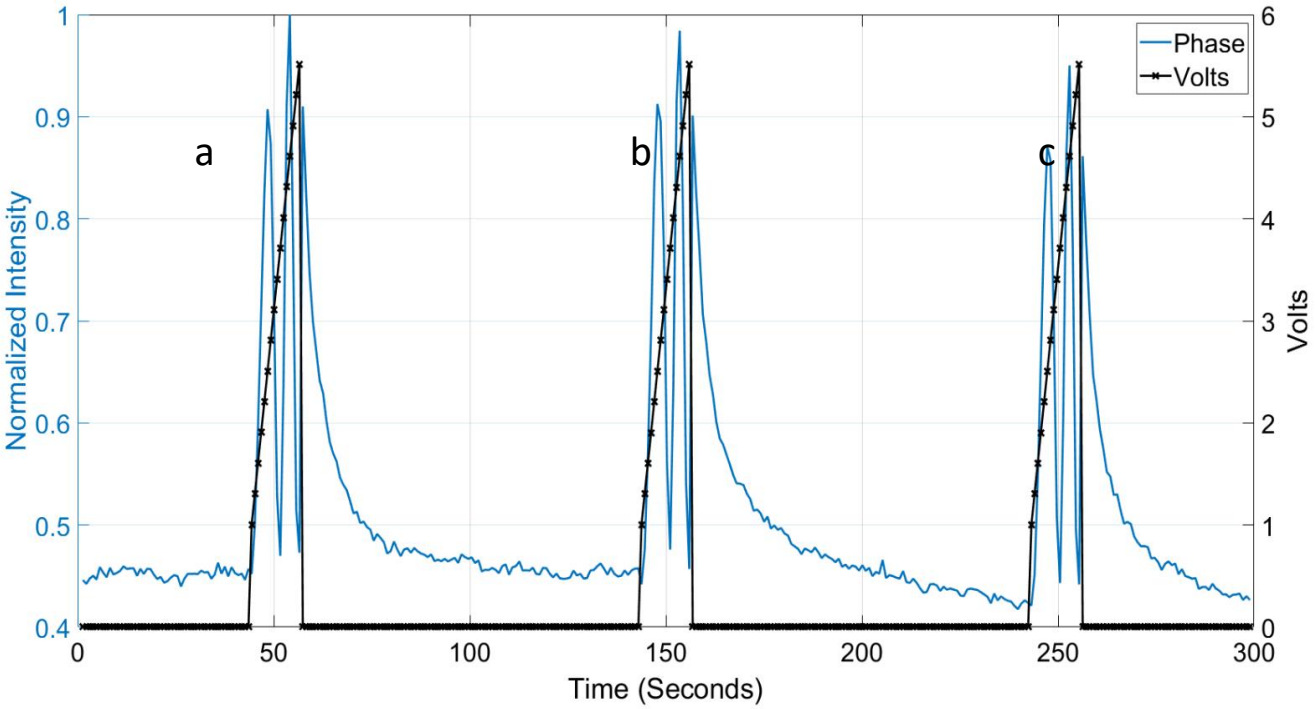

Figure 4.9. Repeatability of phase shift. Z-plot of a One image is captured at each voltage step (0.3V), an image stack is formed anda z-profile of one of the bead is plotted against time

4.3.3 Phase shift according to wavelength, polarization and sensing arm length

Next three experiments will provide information about how much powers is needed for phase change in each polarization mode, how it relates to the length of the micro-heater and the wavelength of light.

Polarization and wavelength experiment were investigated using 0.5cm sensing length interferometer. Phase change dependency on sensing length experiment was performed using both 0.5cm and 1cm sensing length. Both of these interferometers have the same interference angle ($sin\alpha = 30°$). However, phase change does not depend on interference angle.

Temperature change in PDMS is proportional to the power a micro-heater takes. This temperature change causes phase change in a thermo-optical phase modulator. Phase change depends on the thermo-optic coefficient of the material, wavelength, polarization of light and the length of the heat sensing arm, which can be written as equation 4.1. [22].

$$\frac{\partial \varphi}{\partial T} = 2\pi L * \frac{\partial n_{eff}}{\partial n} * \frac{\partial n}{\partial T} \qquad (4.1)$$

$\frac{\partial \mathrm{n_{eff}}}{\partial \mathrm{n}}$ Value depends on wavelength and polarization mode, Table 4.4 shows the result form the simulation done by Dr. Firehun Tsige Dullo. L Is the Length of the heat sensing arm. And $\frac{\partial \mathrm{n}}{\partial \mathrm{T}} = -4.2 \times 10^{-4}\ \mathrm{RIU/K}$ [23], thermo-optic coefficient of the refractive index for PDMS, negative value indicates that the refractive index decreases with increased temperature.

Wavelength (nm)	Polarization	$\frac{dn_{eff}}{dn}$
640	TE	0.156
	TM	0.223
561	TE	0.129
	TM	0.183

Table 4.4 Simulated $\frac{\partial n_{eff}}{\partial n}$ value for TE and TM mode

Using $\frac{\partial \mathrm{n_{eff}}}{\partial \mathrm{n}}$ values from Table 4.4 and table (2) phase change can be estimated:

- $561nm$, TM mode should take around 20% more power for the same amount of phase shift than $640nm, TM$.
- For the same wavelength TE mode needs about 40% more power than TM
- When the wavelength and polarization are same shorter heat sensing length would require twice the power, as the phase change scales linearly with the sensing length (Eq.2).

Phase shift according to the wavelength

In Fig 4.10 normalize bead intensity of two beads are plotted against power, one bead from 640nm and the other from 561nm, both are with TM mod. Each curve is normalised by its maximum value. Bead intensity change corresponds to the phase change. Blue curve shows phase change for 561nm, ($\approx 2\pi$) and the black dashed (- - -) curve represents phase change for 640nm, ($\approx 2\pi$). Smoothing curves are fitted to original curves using 'Smoothing Spline' function in Matlab. For both wavelengths, voltage steps are same, from 0 to 1 then 1 to 5.5V in steps of 0.3V. Power at each step is calculated by multiplying supply voltage with the current that micro heater takes, which are indicated by the circular and triangular markers.

For 640nm (black dashed curve), both π phase change takes $\approx$ 0.185 W, first one from 0.04W to 0.225W and the second one from 0.225W to 0.41W. Phase change shows linear behaviour.

For 561nm (blue continuous curve), it takes $\approx$0.23W for one π shift, which is around 24% more than 640nm, TM.

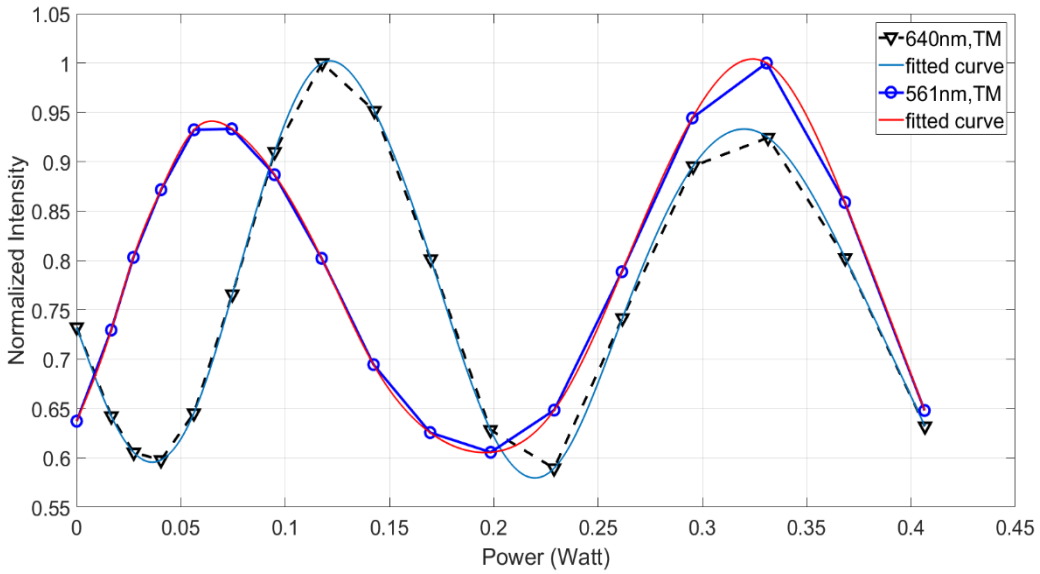

Figure 4.10. Phase shift according to the wavelength. Bead intensity change is plotted against power, which corresponds to the phase change. Same polarization mode is used for both experiment but the wavelengths are different. Blue solid curve is 561nm, TM mode and black dashed curve represents 640nm. TM

Phase shift according to the polarization

Fig 4.11 shows the phase shifting property according to the polarization. In this experiment wavelengths are same (640nm) but the polarization is different. Both results are normalised and plotted against the power. Blue curve represents phase shift for TE polarization and the black dashed curve shows the result for TM mode. Markers indicate power at each point. From analytical solution a total π change for TE mode takes around 42% more power than TM mode. However, this graph does not agree with the analytical results, it shows almost 4 times more power is needed for TE mode.

This has happened possibly due of under-sampling. For TM mode voltage was applied by stepping from 0 to 1 volt, then 1 to 5.5 volts in steps of 0.3V. However, for TE mode no phase shift was observed at that voltage range. So, new voltage range was set for TE mode, from 0 to 1 volt, then 1 to 8.5 volts. This was done to keep the total time of the number of steps below 15 seconds (as discussed in cross-heating section). In the process, steps size got bigger and the effect of under sampling was not obvious until the post image processing.

Another point should be noted, the cross-heating experiment was conducted up to 4 volts. It is highly likely that the heat transfer happens much faster at voltage above 4V.

Due to the time limitation, no further experiments were done for this measurement. In future, these experiments should be repeated to confirm these experimental results.

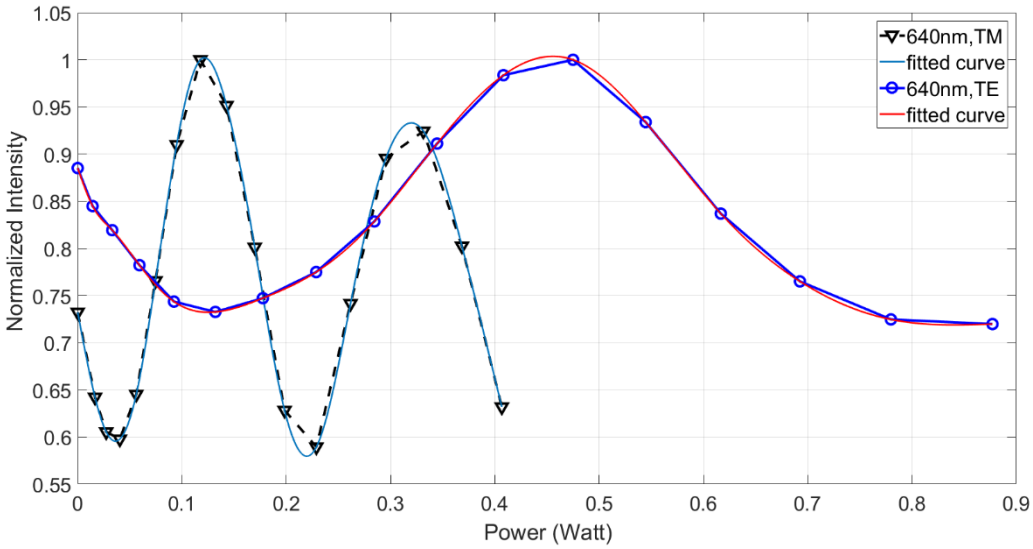

Figure 4.11. Phase shift according to the polarization. Blue solid curve and the black dashed curve represents TE and TM mode respectively. Phase change for TE mode takes more power than TM

Phase shift according to the length of the heat sensing arm

Fig 4.12 shows the phase shifting property according to the length of the heat sensing arm. Both normalised curves are plotted against power. For both plot same wavelength and polarization is used (640nm, TE), but the heat sensing lengths are different 0.5cm and 1cm. Markers indicate the power at each point. Blue curve shows phase shift for 0.5cm length and the black dashed curve for 1cm length. 0.5cm data was obtained from the previous experiment, and one new measurement was taken for the 1 cm length.

For 0.5 cm voltage steps were 0to1 volt, then 1 to8.5 volts in steps of 0.5 volt. With the same voltage range a total π phase shift was observed. Because 1 cm length needs more current to heat up. Then few random voltage ranges were selected and from 5 to 11 volts showed significant phase change and the data was recorded, which is shown in black dashed curve. For the 0.5cm length, voltage steps size were 0.5 volts. With the new voltage range (5to 11V), voltage step size for 1 cm length become 0.4 volt which is close to the value used in the first experiment (phase according to the wavelength).

If we assume that the new result for the 1cm length is correct (sufficient sampling) and for 0.5cm was under sampled then we can conclude that the required power for a full π change in 1cm length is less than that of 0.5cm.

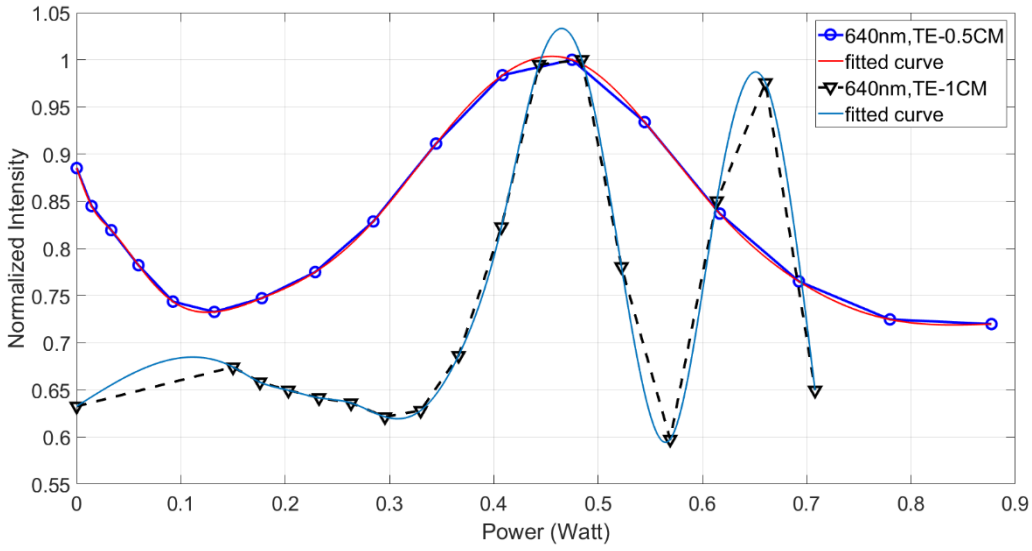

Figure 4.12. Phase shift according to the heat sensing length. For both cure wavelength and polarization more are same, but the heat sensing length is different. Blue curve represents phase change for 0.5cm and the black dashed curve for 1cm sensing length. Phase change takes half the power when heat sensing length doubles

4.3.4 Phase stepping for SIM imaging

This experiment was performed to show that phase stepping can be done with this chip. Fig shows phase stepping for SIM using fluorescent dye (CMDR). For an ideal case SIM uses $0\pi, \frac{2}{3}\pi \; and \frac{4}{3}\pi$ phase steps. This stepping (Fig 4.13) was performed at $0\pi, \frac{1}{3}\pi \; and \frac{2}{3}\pi$ using 1cm length thermo-optics. Power supply was turned on 3 times at, 0 volt, 4.3 volt and 9.6 volt and 3 images were captured. Black blue and red curves represent phase steps at each of these voltage points.

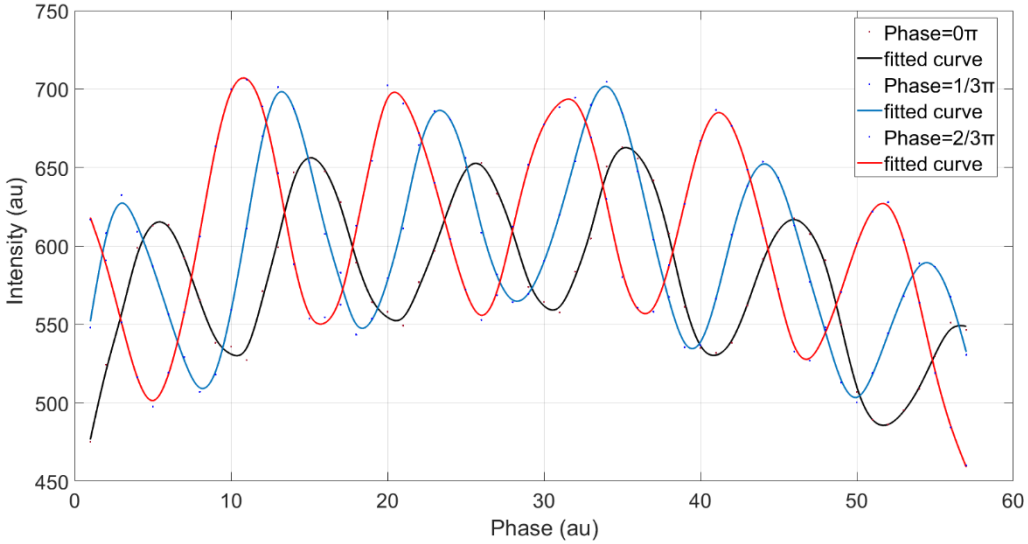

Figure 4.13 Phase stepping for SIM, Each peak in the curve represents each fringe line in the actual fluorescent image. Three images were captured, one at each voltage step. Phase and intensity units are arbitary, black blue and red curves represents phase steps at $0\pi, \frac{1}{3}\pi \; and \frac{2}{3}\pi$. *For ideal case SIM uses* $0\pi, \frac{2}{3}\pi \; and \frac{4}{3}\pi$ *phase steps. This figure confirms that phase stepping can be done using this chip*

5 Conclusion and future work

The main objective of this thesis was to fabricate an on-chip polymer based phase modulator and investigate whether this phase modulator is able to produce required phase shift for SIM imaging. From our experimental result we can conclude that, fabrication of a polymer based phase modulator is achievable using lift-off method. Phase response is fast, has sufficient visibility, repeatable over time and phase stepping is achieved for SIM imaging.

First problem we encountered was the developing time and temperature of the photoresist ma-P 1210. Parameters were optimized and prebaking time of 2 minutes at $80°$ C worked best for our chip. Then there was the problem of surface adhesion between the polymer and the photoresist, PDMS is highly hydrophobic, spin coating photoresist on PDMS failed. So PDMS surface was treated in plasma and good adhesion was achieved. However, adhesion between the two layers was so strong that the lift-off process did not work. Then we tried different plasma treatment time and found that 5 seconds plasma treatment was optimum for our chip. For our lift-off process thickness of silver layer relative to the photoresist was crucial, thickness of $25nm, 50nm\ and\ 100nm$ were tested and $25nm$ produced finest structures. We found out that photoresist crack during fabrication was due to the mismatch between thermal expansion rate of the PDMS and the photoresist. The way around this problem was to increase the baking temperature gradually over 1 minute and cooling slowly over half an hour.

This thermo-optics chip was designed with smaller interference angels ($20°\ and\ 30°$) to be able to capture the interference fringe patterns. We observed that a 60x, 1.2NA objective lens is needed to capture this patterns. Our experimental results of fringe spacing for 640nm wavelength (Table 4.3) show good agreement with the analytical results. However, 561nm results are slightly off due to the aberrations in captured images.

Cross-heating experiment shows that for this particular chip continuous phase modulation time should be limited to 15 seconds, after 15 seconds phase shift measurements might not be reliable.

From our experimental results, required power for a π shift using 640 nm, TM mode is 185mW and for 561nm, TM mode it is 230mW. In TM mode phase starts to change with as little as 20mW power. Which means that the chip is not heated up so much. This is also an advantage when using this chip for live cell imaging.

Whereas, For TE mode phase shift starts at a higher power (≈ 150mW) and total power required for one π shift is considerably more than TM mode. At higher power cross-heating happens much faster. So, when choosing TE mode for future experiments, one should find out the cross-heating time at ≈ 150mW using similar process described in (section 4.4.1) and set the voltage steps accordingly.

From phase change according to the length experiment, we observed that for 1cm length arm, phase shift starts at ≈ 300mW, but the total power it takes for one π shift is approximately half of the power that is needed for 0.5cm.

Considering all these results, we can suggest that for an ideal SIM chip, one should use 640nm, TM mode in combination with shortest possible heat sensing length.

Photoresist crack happened due to CTE mismatch. A possible solution for this problem would be, using a different polymer other than PDMS which matches the thermal coefficient of the photoresist or to find a photoresist which has a similar CTE as PDMS.

We used spin coating technique to coat a uniform layer of PDMS on chip. Which means PDMS fills up the gap between the two arms. Problem of cross heating can be solved in future if we use a micro plotter or a device of same kind which is able to make separate PDMS lines on top of the waveguide.

6 References

1. *Excitation and emission spectra of CellMask plasma stain*. Available from: https://www.thermofisher.com/no/en/home/life-science/cell-analysis/labeling-chemistry/fluorescence-spectraviewer.html?SID=srch-svtool&UID=32721h2o.
2. *Refraction of light at the interface between two media*. Available from: https://en.wikipedia.org/wiki/Total_internal_reflection.
3. A, D., et al., *Sensitive Label-Free Biomolecular Detection Using Thin Silicon Waveguides*. Vol. 2008. 2008.
4. Bahaa E. A. Saleh , M.C.T., *Fundamentals of Photonics, 2nd Edition*. 2nd ed. 2006. 58.
5. Guo, L. and S.P. DeWeerth, *An effective lift-off method for patterning high-density gold interconnects on an elastomeric substrate.* Small (Weinheim an der Bergstrasse, Germany), 2010. **6**(24): p. 2847-2852.
6. Adrega, T. and S.P. Lacour, *Stretchable gold conductors embedded in PDMS and patterned by photolithography: fabrication and electromechanical characterization.* Journal of Micromechanics and Microengineering, 2010. **20**(5): p. 055025.
7. Han-Sheng, C. and W. Steven, *Design, fabrication and characterization of a conducting PDMS for microheaters and temperature sensors.* Journal of Micromechanics and Microengineering, 2009. **19**(4): p. 045010.
8. Balakrisnan, B., S. Patil, and E. Smela, *Patterning PDMS using a combination of wet and dry etching.* Journal of Micromechanics and Microengineering, 2009. **19**(4): p. 047002.
9. Bao, W., et al., *Lithography-free fabrication of high quality substrate-supported and freestanding graphene devices.* Nano Research, 2010. **3**(2): p. 98-102.
10. Chao-Xuan, L. and C. Jin-Woo, *Patterning conductive PDMS nanocomposite in an elastomer using microcontact printing.* Journal of Micromechanics and Microengineering, 2009. **19**(8): p. 085019.
11. Xia, Y. and G.M. Whitesides, *Soft Lithography.* Angewandte Chemie International Edition, 1998. **37**(5): p. 550-575.
12. GmbH, m.r.t. *ma-P 1210 data sheet*. Available from: http://www.microchem.com/PDFs_MRT/ma-P%201200%20overview.pdf.
13. Ltd, O. *Demonstration of Static Dispense Spin Coating to the Edge of the Substrate*. Available from: https://www.ossila.com/pages/demonstration-of-static-dispense-spin-coating-to-the-edge-of-the-substrate.
14. SE, S.M. *SUSS MJB4 datasheet*. Available from: https://www.suss.com/brochures-datasheets/mask-aligner-mjb4.pdf.
15. Bhattacharya, S., et al., *Studies on surface wettability of poly(dimethyl) siloxane (PDMS) and glass under oxygen-plasma treatment and correlation with bond strength.* Journal of Microelectromechanical Systems, 2005. **14**(3): p. 590-597.
16. Ltd, O. *Spin Coating: A Guide to Theory and Techniques*. Available from: https://www.ossila.com/pages/spin-coating.
17. Corning, D. *Sylgard®184 Silicone Elastomer Datasheet*. Available from: http://igem.org/wiki/images/2/29/T--Technion_Israel-HardwarespecsPDMS.pdf.
18. INC, N.I. *Resolution*. Available from: https://www.microscopyu.com/microscopy-basics/resolution.
19. Schindelin, J., et al., *Fiji: an open-source platform for biological-image analysis.* Nature Methods, 2012. **9**: p. 676.
20. *TetraSpeck excitation/emission peaks*. Available from: https://www.thermofisher.com/order/catalog/product/T7279.
21. *Anaconda Distribution Version 5.3*. Available from: https://www.anaconda.com/download/.
22. Dullo, F.T., et al., *Temperature Sensitivity of a Waveguide Young Interferometer.* IEEE Photonics Technology Letters, 2016. **28**(11): p. 1205-1208.
23. Lindecrantz, S.M., et al., *Characterization of a waveguide Mach-Zehnder interferometer using PDMS as a cover layer*. 2015. Vol. 10. 2015.